

# The network architecture of general intelligence in the human connectome

Received: 4 March 2025

Accepted: 18 December 2025

Published online: 26 January 2026

 Check for updates

Ramsey R. Wilcox<sup>1,2,3</sup>, Babak Hemmatian<sup>4</sup>, Lav R. Varshney<sup>4,5</sup> & Aron K. Barbey <sup>1,2,3,6,7,8,9</sup> 

Advances in network neuroscience challenge the view that general intelligence ( $g$ ) emerges from a primary brain region or network. Network Neuroscience Theory (NNT) proposes that  $g$  arises from coordinated activity across the brain's global network architecture. We tested predictions from NNT in 831 healthy young adults from the Human Connectome Project. We jointly modeled the brain's structural topology and intrinsic functional covariation patterns to capture its global topological organization. Our investigation provided evidence that  $g$  (1) engages multiple networks, supporting the principle of distributed processing; (2) relies on weak, long-range connections, emphasizing an efficient and globally coordinated network; (3) recruits regions that orchestrate network interactions, supporting the role of modal control in driving global activity; and (4) depends on a small-world architecture for system-wide communication. These results support a shift in perspective from prevailing localist models to a theory that grounds intelligence in the global topology of the human connectome.

General intelligence ( $g$ ) captures the remarkable human capacity to find solutions for the diverse problems faced in life, accounting for performance across a wide range of academic, professional, social, and health contexts<sup>1</sup>. The pervasive predictive power of  $g$  motivates the study of its cognitive and neurobiological foundations, an interdisciplinary endeavor that addresses one of the most fundamental and enduring questions in modern science: How does the human brain create general intelligence? Prevailing theories argue that intelligence arises from individual differences in the function of a specific cortical region<sup>2</sup> or network<sup>3</sup>. For example, proponents of the Parieto-frontal integration theory (P-FIT) posit that a discrete parieto-frontal network underlies human intelligence, emphasizing the role of this network in the generation and testing of hypotheses for problem solving<sup>3</sup>. Despite the success of functionally localized models, recent advances in network neuroscience motivate an alternative perspective, highlighting the importance of the brain's global network architecture as proposed

by the Network Neuroscience Theory<sup>4</sup> (NNT). According to this framework, general intelligence reflects individual differences in system-wide mechanisms for efficient and flexible information processing.

Network Neuroscience Theory predicts that intelligence emerges from four key properties of the human connectome. First, it relies on distributed processing across diverse brain networks, reflecting NNT's core principle that  $g$  does not originate from a primary cortical region or network. Accumulating evidence in network neuroscience supports this view, demonstrating that whole-brain functional connectivity models more accurately predict intelligence than models based on any single network<sup>5,6</sup>. Recent evidence further suggests that the superior performance of whole-brain models reflects the engagement of between-network connections that enable system-wide communication and dynamics<sup>7</sup>. New methods to jointly model the structural and functional connectome capture such communications more effectively by allowing structural and functional information to inform each

<sup>1</sup>Decision Neuroscience Laboratory, University of Notre Dame, Notre Dame, IN, USA. <sup>2</sup>Notre Dame Human Neuroimaging Center, University of Notre Dame, Notre Dame, IN, USA. <sup>3</sup>Department of Psychology, University of Notre Dame, Notre Dame, IN, USA. <sup>4</sup>AI Innovation Institute, Stony Brook University, Stony Brook, NY, USA. <sup>5</sup>Department of Electrical & Computer Engineering, University of Illinois, Urbana, IL, USA. <sup>6</sup>Department of Psychology, University of Illinois, Urbana, IL, USA. <sup>7</sup>Department of Bioengineering, University of Illinois, Urbana, IL, USA. <sup>8</sup>Beckman Institute, University of Illinois, Urbana, IL, USA. <sup>9</sup>Institute for Defense Analyses, Alexandria, VA, USA. ✉ e-mail: [abarbey@nd.edu](mailto:abarbey@nd.edu)

other in the estimation of the brain's global topology<sup>8</sup>. This enables a more comprehensive analysis of the relationship between the brain's global network organization and human intelligence.

Second, NNT predicts that global network communication depends on the engagement of weak, long-range connections (i.e., weak ties). Prior research demonstrates that weak ties support the efficient transfer of information between networks, enabling system-wide communication and dynamics<sup>9</sup>. This adaptability is essential for intelligence, which often involves solving novel problems or responding to unexpected challenges. Weak connections are more readily modulated by ongoing neural activity and therefore allow for dynamic reconfiguration of brain networks to adapt to changing task demands. Indeed, prior research suggests that weak ties predict individual differences in general intelligence<sup>10</sup>, providing a globally efficient architecture for the flexible recruitment of brain networks<sup>11–14</sup>. According to NNT, weak, long-range connections serve as the neural infrastructure for system-wide network communication and flexibility, enabling the capacity for intelligent thought and action. While the role of weak ties in general intelligence has been examined with respect to functional connectivity, research using modern joint structure-function modeling techniques, which provide a more comprehensive characterization of the brain's global topology, has yet to be conducted.

Third, NNT proposes that global network communication relies on specialized modal control regions that orchestrate system-wide function<sup>15–17</sup>. These regions are located such that they enable access to diverse functional states, including those not readily accessible through typical network interactions (i.e., difficult-to-reach states). According to this view, modal control regions act as network drivers, dynamically steering the configuration of brain networks towards states that enable goal-directed behavior and adaptive decision making<sup>18–20</sup>. Recent evidence demonstrates a positive correlation between the flexibility afforded by modal control regions and performance in complex problem-solving tasks<sup>19,20</sup>. The capacity of modal control regions to drive the configuration of brain networks is known to facilitate problem-solving by enabling the integration of information from diverse and potentially distant brain regions. This integration is critical for tasks requiring the coordination of multiple cognitive processes, a hallmark of general intelligence. Therefore, the capacity of modal control regions to flexibly navigate a broad repertoire of brain states is theorized to be an essential factor underlying general intelligence according to NNT<sup>4</sup>. The link between modal control and intelligence, however, remains unexplored in prior work.

Finally, the proposed network properties of intelligence, which emphasize a locally efficient and globally coordinated system, are predicted to emerge from a small-world topology. This unique topology incorporates both high local clustering and global communication via short topological path lengths. Thus, small-world networks enable both local and global efficiency by balancing two opposing system-wide principles. The first principle is segregation, a fundamental organizing principle that promotes specialization of function while minimizing wiring costs. This is achieved by dividing the cortex into distinct anatomical modules constructed from densely clustered nodes. This modular organization allows for independent processing of specific cognitive tasks and reduces the average length of axonal connections, ultimately enhancing signal transmission speed<sup>21</sup>. The second principle is integration, which enables system-wide network communication. This is achieved through long-range connections. These connections come at a cost, requiring more resources (i.e., higher wiring cost), but they create shorter topological pathways for efficient information exchange across the entire system. A small-world topology provides a balance between efficient local processing and flexible integration of information across the connectome<sup>22,23</sup>. While prior research has examined the relationship between  $g$  and measures

of network integration<sup>24</sup> and segregation<sup>25</sup>, the predicted role of a small-world topology in intelligence remains to be examined.

The present study investigates the core predictions of NNT in a sample of healthy young adults ( $N = 831$ ) from the Human Connectome Project, examining whether general intelligence: (1) engages multiple brain networks, supporting the theory's principle of distributed processing; (2) relies on weak, long-range connections, reflecting the theory's emphasis on a globally coordinated network architecture; (3) recruits regions that orchestrate network interactions, supporting the predicted role of modal control regions that drive global activity; and (4) has a small-world topology, central to the efficiency and flexibility of global information processing, and the predicted architecture for system-wide network communication and dynamics. We employed a comprehensive battery of cognitive tests to derive a latent  $g$  factor and assess its relationship with resting-state functional magnetic resonance imaging (rs-fMRI) and diffusion-weighted magnetic resonance imaging (dw-MRI) to investigate the network architecture of intelligence.

To this end, we applied methodological advances in network modeling to integrate structural connectivity data, derived from diffusion-weighted tractography, with functional co-activation patterns, derived from resting-state independent component analysis (ICA), in a data-driven manner. The result is a whole-brain, multi-modal connectome that describes the capacity of structural connections to transfer functional information<sup>8</sup>. This approach reflects the following methodological innovations that enable a rigorous investigation of NNT's core predictions.

First, ICA measures the dynamics of the brain's functional organization by extracting distinct neuronal co-activation patterns across the cortex. Each pattern contains strong functional contributions from a set of brain regions that represent an intrinsic connectivity network (ICN). Additionally, each component may also contain weaker functional contributions from regions outside its core ICN. These weak contributions reflect the integrative nature of the brain's topology and the ability of regions belonging to separate networks to transiently communicate with each other. Thus, the employed ICA method not only captures within-network communication patterns but also between-network communications where cortical regions flexibly alter their network affiliation.

Second, the integrative nature of the model is designed to correct for well-known issues in the underestimation of white-matter tracts that traverse cross-fiber areas<sup>26</sup>. By jointly modeling structure and function, this approach ensures that connections between regions are strong enough to support their observed patterns of co-activation. Thus, the weak, long-range connections that are central to testing NNT's predictions may be recovered that structural data alone might miss.

Finally, a multi-modal approach enables a more comprehensive investigation of the NNT framework. A growing body of evidence demonstrates that the brain's structural topology shapes the efficiency of communication between brain regions<sup>19,27,28</sup>, ultimately influencing the functional dynamics of intelligence. Integrating structural and functional connections in a data-driven manner offers a deeper understanding of the neural mechanisms underlying intelligence by more accurately estimating the brain's global topology (e.g., to capture such features as weak ties).

In summary, the NNT framework challenges the prevailing view of intelligence as localized within a primary brain region<sup>2</sup> or network<sup>3</sup>, emphasizing instead the importance of system-wide communication and dynamics. The present study investigated the novel predictions of the NNT framework within an integrated analysis approach that (1) jointly models the brain's structural connectome with intrinsic sources of functional covariation, (2) derives modal control metrics, and (3) examines small-worldness in the prediction of general intelligence. To further validate the NNT framework, we conducted a conceptual

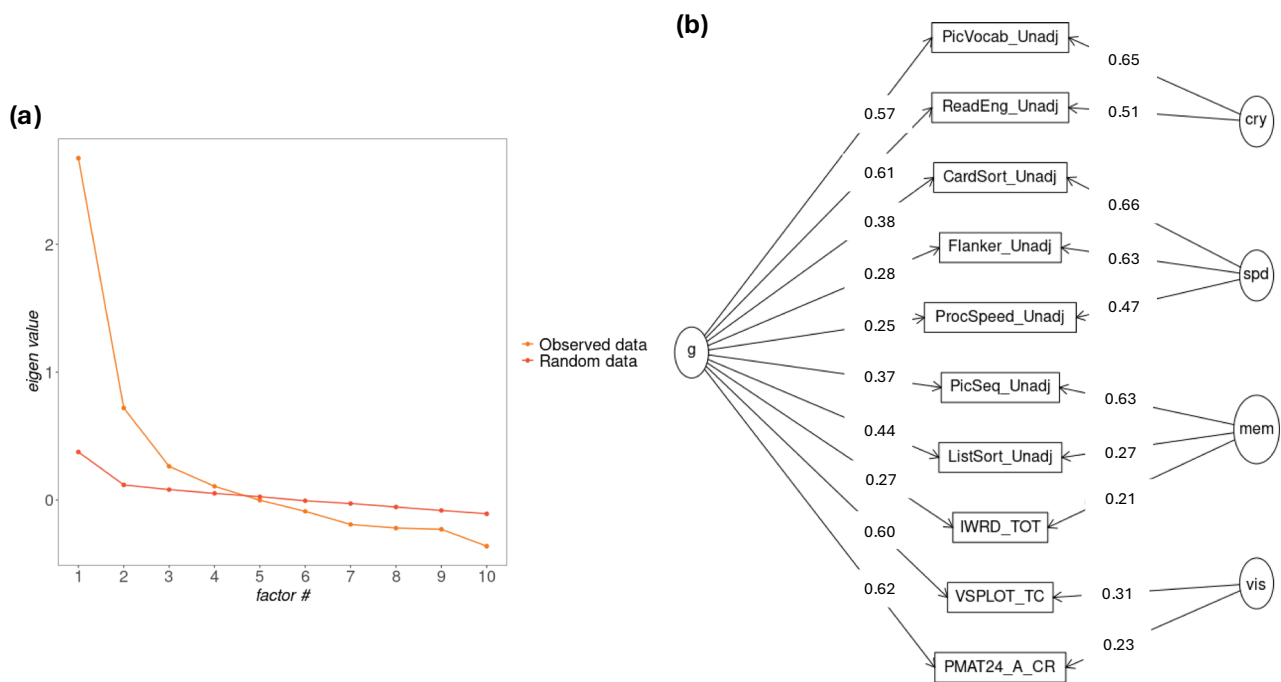


**Fig. 1 | Results of the factor analysis used to generate subject-level *g* scores.** **a** Plot of Horn's parallel analysis describing the eigenvalues for each component calculated from the observed data against the eigenvalues calculated from random data. The orange line represents eigenvalues from the actual dataset. The red line represents average eigenvalues from the random datasets. **b** A schematic of the bi-

factor model. The rectangles identify the tests included. Loading values are overlaid on straight links. Latent factors are contained in ellipses (*g*: a latent, common factor among the group factors; *cry*: a latent crystallized ability factor; *spd*: a latent processing speed factor; *mem*: a latent memory factor; *vis*: a latent visuo-spatial ability factor).

replication to assess the generalizability of our findings in an independent sample of 145 participants (see Supplemental Materials). Results from two independent studies with a combined sample of 976 participants validate the predictions of NNT and call for a shift in perspective from prevailing localist models towards a framework that grounds intelligence in the global topology and dynamics of the human connectome.

## Results

### Estimating general intelligence from psychometric *g*

Horn's parallel analysis found the eigenvalue of four latent factors to be significantly higher than the eigenvalues of their random dataset counterparts (Fig. 1a). Thus, we included four group factors in our bifactor model (Fig. 1b), interpreted as crystallized ability (PicVocab, ReadEng), processing speed (CardSort, Flanker, ProcSpeed), visuo-spatial ability (VSPLIT\_TC, PMAT24\_A\_CR), and memory (PicSeq, ListSort, IWRD\_TOT). These group labels are intuitive and coincide with prior studies that adopted the same approach<sup>6</sup>. The model exhibited indices of good fit with a high comparative fit index (CFI = 0.99) and low root mean square error of approximation (RMSEA = 0.03). Statistical practices identify CFI values above 0.95, and RMSEA values lower than 0.05 as indicating good fit<sup>29</sup>. The *g* factor accounted for 58.72% of the total variance.

### General intelligence depends on a global network architecture

Consistent with the predictions of NNT, a whole-brain, connectome-based predictive model (CPM) reliably predicted out-of-sample *g* scores (Fig. 2a), explaining a significant proportion of the variance ( $R^2 = 0.12$ ;  $p_{1000} = 0.001$ ; Fig. 2c) and yielding a significant correlation between predicted and observed *g* scores ( $r = 0.35$ ;  $P_{1000} = 0.001$ ; Fig. 2b). The observed *nRMSD* was significantly lower than the value obtained from a null distribution ( $nRMSD = 0.94$ ;  $P_{1000} = 0.001$ ; Fig. 2d).

### General intelligence is constructed from multiple brain networks and their interactions

Consistent with the predictions of NNT, inclusion analyses demonstrated that the independent predictive power of each ICN was lower than the whole-brain model (Fig. 3a). Nonetheless, the results revealed different relationships with *g* across the 12 ICNs. As might be expected, the fronto-parietal network (FPN) exhibited the highest independent predictive power ( $R^2 = 0.056$ ). The auditory network (AUD) followed and exceeded all other networks ( $R^2 = 0.054$ ). The default mode (DMN), somatomotor (SMN), and dorsal attention (DAN) networks all exhibited similar predictive power ( $R^2 = [0.043-0.047]$ ). The cingulo-opercular (CON) and language (LAN) networks were also similar to each other ( $R^2 = 0.031$ ,  $R^2 = 0.025$ ), while the primary (V1) and secondary (V2) visual networks exhibited the lowest predictive power ( $R^2 = 0.008$ ,  $R^2 = 0.006$ ). The orbito-affective (OA), posterior multi-modal (PMM), and ventral multi-modal (VMM) networks did not contain enough connections that survived the feature selection step across all five folds for an elastic net model to be fit. Thus, they did not have any resulting performance metric. Despite the differences in predictive power across ICNs, the exclusion analyses showed that when each network is removed from the whole-brain model, the change in performance is negligent (Fig. 3b). This suggests that between-network interactions primarily drive the prediction of *g* scores.

To confirm that predictive performance relies primarily on between-network connections, we plotted on glass brains only those connections that were predictive (i.e., survived feature selection) and highly stable across participants (i.e., survived across all 5 folds; Fig. 4). When examining these graphs, a globally distributed and interactive picture emerges. Large networks, like CON, FPN, and DMN, exhibit many between-network connections, with graphs so dense and distributed as to obfuscate any coherent local pattern. We see similarly distributed and interactive, albeit less dense, graphs for smaller

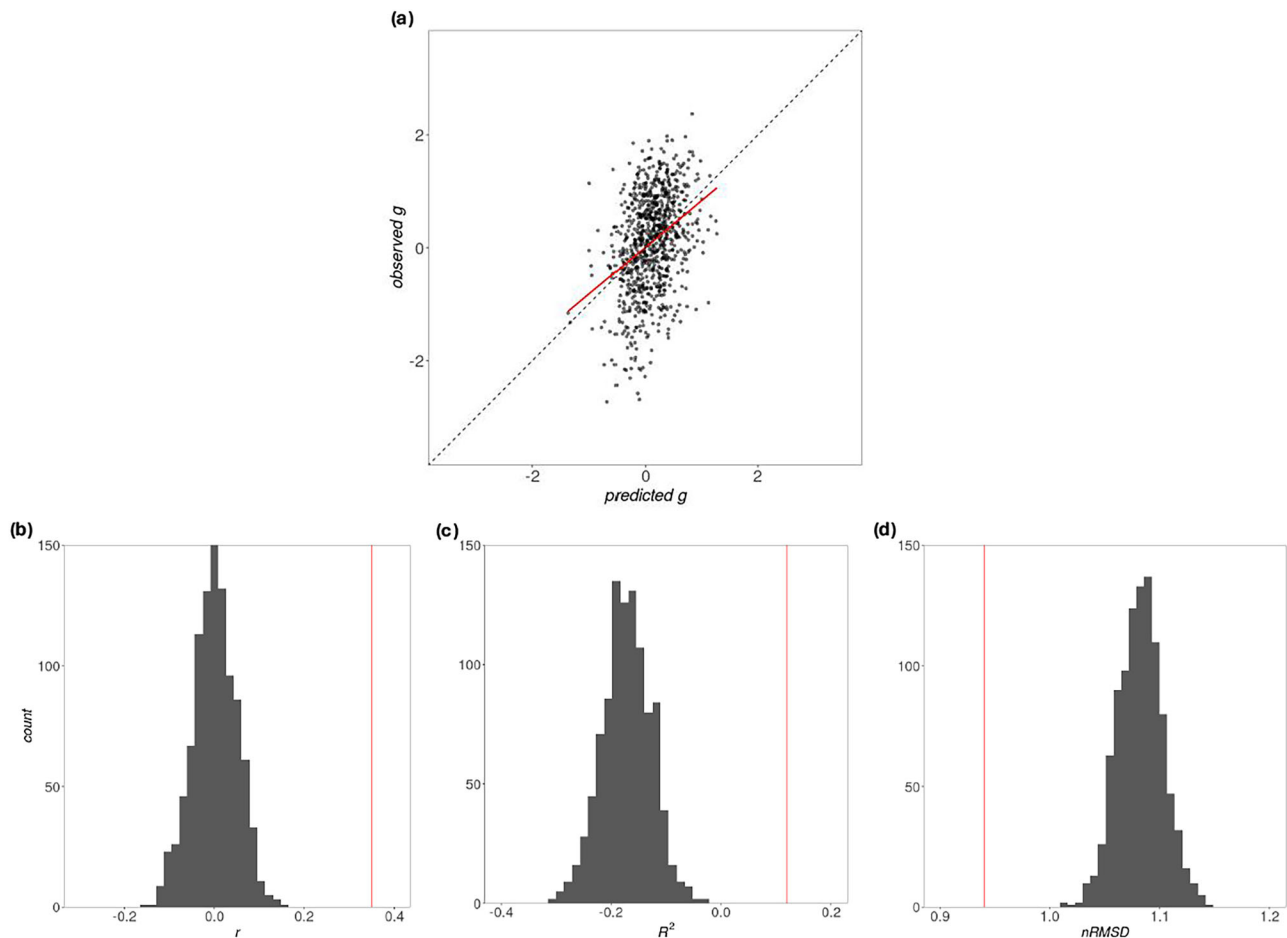


**Fig. 2 | Joint structure-function brain connections across the entire cortex reliably predict general intelligence. a** Scatterplot of predicted  $g$  scores compared to observed  $g$  scores. ( $r = 0.35$ ,  $p_{1000} = 0.001$ ;  $R^2 = 0.12$ ,  $p_{1000} = 0.001$ ;  $nRMSD = 0.94$ ,  $p_{1000} = 0.001$ ). The red line denotes the regression line. The dashed black line denotes an identity line. As expected with a model of good fit, the

regression line approaches the identity line. **b–d** The permutation tests of performance metrics with 1000 randomly shuffled datasets used to establish significance with respect to an empirically derived null distribution. Red lines represent statistical values from the whole-brain model, while bars collectively represent the distribution of values across the random permutations.

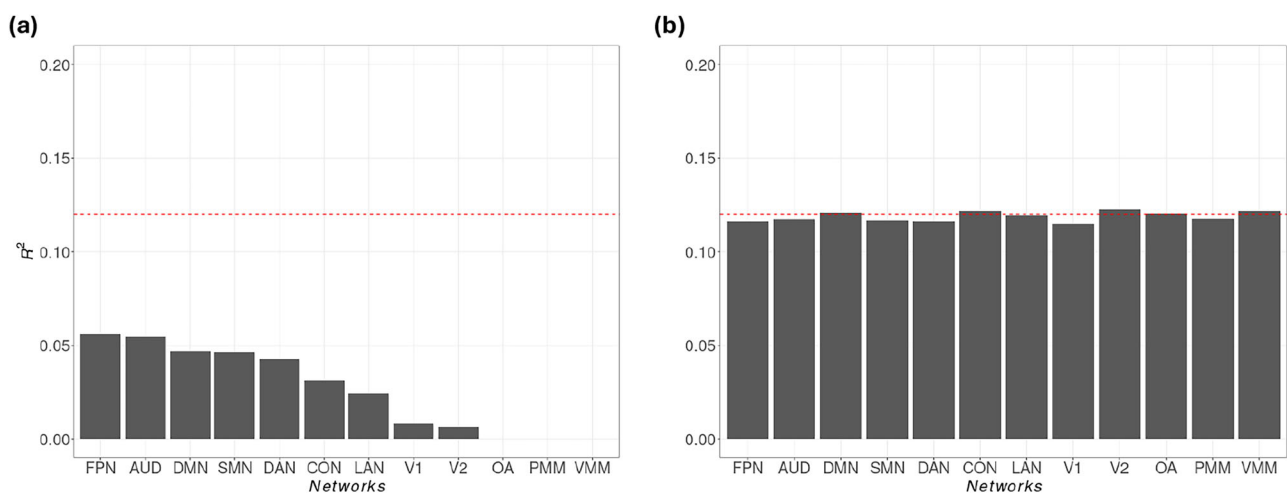


**Fig. 3 | Lesion analyses examining the predictive performance of the individual ICNs.** The red dotted line in graphs **a**, **b** represents the whole-brain model performance. **a** Results from the inclusion analysis, where predictive performance was evaluated for connections originating from each ICN. **b** Results from the exclusion analysis, where predictive performance was evaluated for the whole-brain model with each ICN removed, respectively. V1 Primary Visual Network,

V2 Secondary Visual Network, SMN Somatomotor Network, CON Cingulo-opercular Network, DAN Dorsal Attention Network, LAN Language Network, FPN Fronto-parietal network, AUD Auditory Network, DMN Default Mode Network, PMM Posterior Multi-modal Network, VMM Ventral Multi-modal Network, OA Orbito-affective Network.

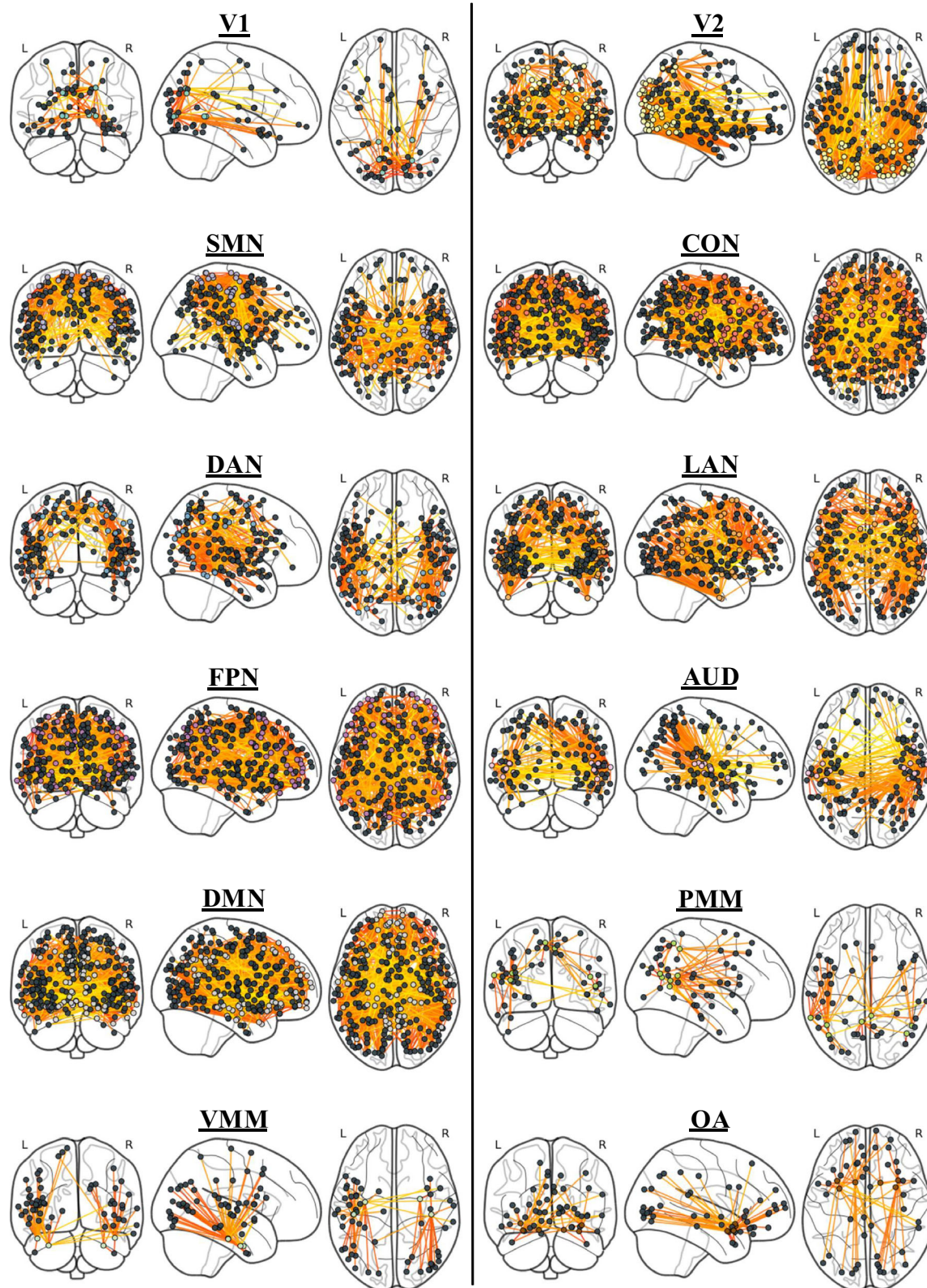


**Fig. 4 | Predictive connections that survived feature selection for all five folds plotted on glass brains.** Graphs are organized according to the ICN origin of connections, where connections reside within a given ICN and between that ICN and the remaining eleven networks. Nodes within the ICN of interest are colored for each graph, while nodes outside the ICN of interest are black. Brighter edges denote weaker connections, while darker edges denote stronger connections. V1 =

Primary Visual Network, V2 = Secondary Visual Network, SMN = Somatomotor Network, CON = Cingulo-opercular Network, DAN = Dorsal Attention Network, LAN = Language Network, FPN = Fronto-parietal Network, AUD = Auditory Network, DMN = Default Mode Network, PMM = Posterior Multi-modal Network, VMM = Ventral Multi-modal Network, OA = Orbito-affective Network.

networks. For example, the V1, AUD, and OA all exhibited connections between networks and distributed across the whole cortex. The AUD was particularly interactive, demonstrating many inter-hemispheric connections, whereas the V1 and OA tended to only present a few inter-hemispheric connections. The VMM and PMM graphs also exhibited distributed and interactive behavior, but to a lesser degree, demonstrating few connections with the frontal cortex. Medium-sized networks, such as V2, DAN, SMN, and LAN, displayed patterns similar to large networks but also somewhat less dense.

It is noteworthy that networks that lacked significant connections within their own boundaries (OA, PMM, VMM) nonetheless exhibited predictive between-network connections. These findings collectively support a globally integrated network architecture for intelligence, characterized by distributed information processing, with between-network communication playing a critical role.

### Feature set size bias

It is critical to verify that the predictive efficacy of the whole-brain model compared to smaller, localized models (i.e., inclusion models) was not an artifact of its larger feature set. To examine this issue, we conducted a permutation-based control analysis within our previously described predictive modeling framework. Specifically, we performed a grid search across feature sets of increasing size, each populated with randomly permuted connections to isolate the effect of feature dimensionality. Our results (Fig. 5) demonstrate that increasing the number of input features does not improve predictive accuracy as measured by a Pearson correlation ( $r_{\text{Pearson correlation vs. set size}} = -0.081$  [-0.232, 0.075],  $t(159) = -1.021$ ,  $p = 0.309$ ; Fig. 5a) and coefficient of determination ( $r_{\text{coefficient of determination vs. set size}} = -0.724$  [-0.790, -0.641],  $t(159) = -13.22$ ,  $p < 2.2 \times 10^{-16}$ \*\*\*; Fig. 5b). In fact, we show that larger feature sets can lead to decreases in performance compared to smaller sets (Fig. 5b). This finding highlights an important methodological point: Pearson correlations between observed and predicted values in a cross-validation framework can provide misleading estimators of model performance. Thus, it is essential to include less biased metrics, such as the coefficient of determination ( $R^2$ ), for robust model assessment.

### General intelligence depends on weak, long-range connections

We examined whether significant connections that tended to be weaker in higher  $g$  individuals, compared to lower  $g$  individuals, were longer than those that tended to be stronger. Given connections were standardized (i.e., z-scored) before model fitting, the sign of their associated beta coefficients describes whether a connection is weaker in high  $g$  individuals (i.e., negatively related) or stronger in high  $g$  individuals (i.e., positively related). Given this standardization, we expect weak ties to exhibit negative beta coefficients, which were used to group features by direction of outcome association (i.e., negatively or positively related to  $g$ ). The mean distance of predictive connections was significantly higher for connections negatively related to  $g$  compared to those positively related to  $g$  ( $M_{\text{pos}} = 105.20$  mm,  $SE_{\text{pos}} = 1.05$  mm,  $M_{\text{neg}} = 151.20$ ,  $SE_{\text{neg}} = 2.04$ ,  $W = 520005$ ,  $p < 0.0001$ ). This demonstrates that predictive connections weak in strength tend to be longer in distance. As Fig. 6a illustrates, this is not due to outliers but reflects the general distribution of connection distance.

To further investigate the importance of weak, long-range connections with  $g$ , we examined whether Haufe coefficients, measures of feature importance for an outcome, changed as a function of connection length, and if this is moderated by direction of outcome association. That is, for a weak tie, is it the case that it is more important for  $g$  when it is longer in distance than other weak ties? As our regression model reveals, this is indeed the case (Table 1). Figure 6b provides an illustration of this moderated relationship between the distance of positively and negatively related connections and their Haufe coefficients. For positively related connections, the opposite

trend is seen, where strong ties that are shorter in distance are more important for  $g$  compared to other strong ties. Correlation tests between Haufe coefficients and distance, independently carried out in positively and negatively related connections, confirmed these findings ( $r_{\text{negative}} = -0.449$  [-0.527, -0.364],  $t(371) = -9.683$ ,  $p < 0.0001$ \*\*\*;  $r_{\text{positive}} = -0.145$  [-0.190, -0.099],  $t(1786) = -6.179$ ,  $p < 0.0001$ \*\*\*). Thus, higher  $g$  individuals tend to exhibit weaker connections longer in distance and stronger connections shorter in distance compared to lower  $g$  individuals. Taken together, these findings validate the predictions of NNT, demonstrating that general intelligence depends on weak ties.

### General intelligence depends on modal control regions

We fit an MDMR model to examine the relationship between  $g$  and cortical modal control profiles. We found that  $g$  significantly related to the modal control profile of participants ( $F_{\text{observed}} = 2.807$ ,  $\bar{F}_{\text{permutation}} = 1.003$ ,  $SD_{\text{permutation}} = 0.27$ ,  $p_{1000} = 0.001$ ; Fig. 7a), suggesting that  $g$  depends on the global orchestration of brain functions. Modal control values were differentially distributed across all 12 networks (Fig. 7b). The DMN contained the most regions after excluding those in the bottom 25th percentile (22.963%). CON and V2 networks displayed similar region proportions, higher than the remaining networks (16.667% and 15.556%, respectively). The FPN also displayed a somewhat larger proportion (11.481%) compared to most networks. The SMN, LAN, DAN, and AUD all displayed low proportions (8.519%, 7.407%, 6.296%, and 5.556%, respectively). Finally, the PMM, V1, OA, and VMM all displayed very low proportions (1.852%, 1.481%, 1.481%, and 0.741%, respectively). These proportions align with the overall size of the ICNs apart from V2, whereby larger ICNs have greater representation in the set of nodes with the highest values of modal control. As Fig. 6c illustrates, regions with high modal control values (i.e., reddish regions) were distributed across the frontal, parietal, cingulate, and temporal cortices. The CON, FPN, DMN, AUD, V2, and OA all seemed to display high modal control values (see Fig. 7d for network assignments). This pattern of findings supports the predictions of NNT, demonstrating that general intelligence depends on the brain's capacity to engage modal control mechanisms that orchestrate network activity.

### General intelligence depends on a small-world topology

The Telesford metric of small-worldness was used to investigate the relationship between this unique topology, one that balances high local clustering, with global integration via short path lengths, and  $g$ . Values close to 0 denote greater small-worldness, values closer to 1 indicate a deviation towards a more random network, and values closer to -1 indicate a deviation towards a more regular network. No participants exhibited a deviation towards a locally integrated, globally segregated regular network. As predicted, individuals with higher  $g$  scores exhibited greater small-worldness than individuals with lower  $g$  scores ( $r = -0.204$  [-0.268, -0.137],  $t(829) = -5.986$ ,  $p < 0.0001$ \*\*\*; Fig. 8a). Complementary analyses examining the topological properties that underlie small-worldness (i.e., average shortest path length and average local clustering) provided additional insight into this relationship. Individuals with higher  $g$  scores exhibited higher local clustering ( $r = 0.143$  [0.076, 0.209],  $t(829) = 4.174$ ,  $p < 0.0004$ \*\*\*; Fig. 8b.) and shorter average path lengths ( $r = -0.079$  [-0.146, -0.011],  $t(829) = -2.274$ ,  $p = 0.023$ \*; Fig. 8c). This suggests highly integrated local clusters combined with inter-cluster connections that allow for the efficient sharing of information are important for  $g$ . The observed findings support the NNT framework, providing evidence that intelligence emerges from the brain's small-world organization.

## Discussion

The Network Neuroscience Theory<sup>4</sup> (NNT) posits that general intelligence arises from individual differences in the global topology of the

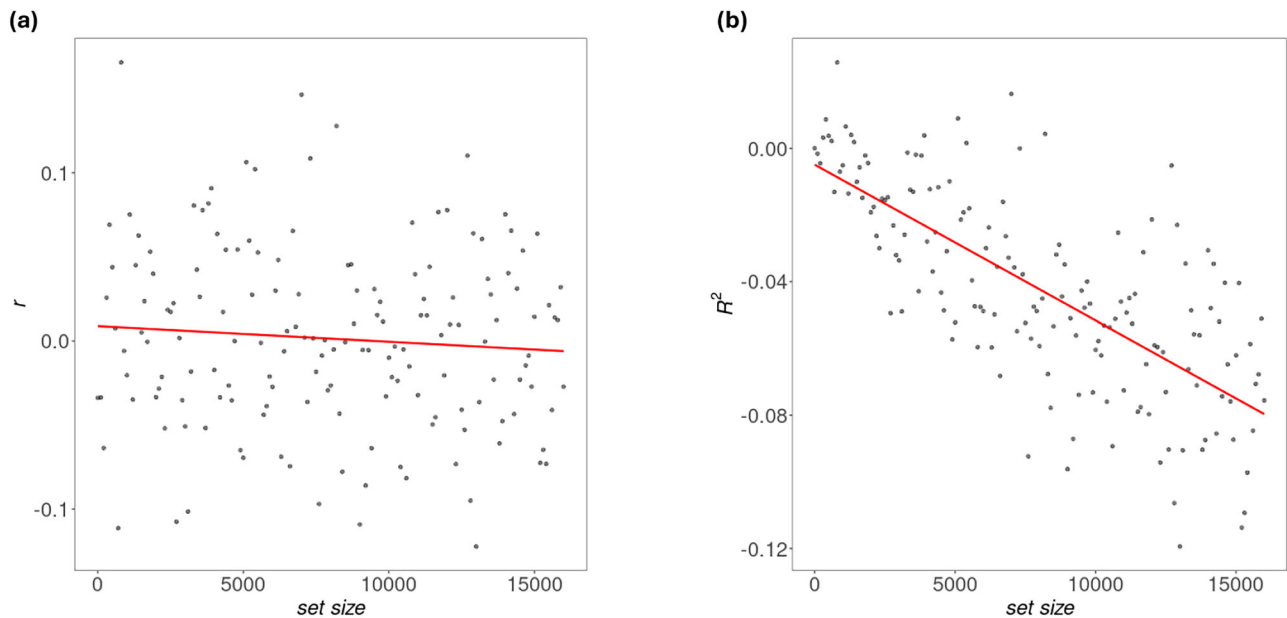


**Fig. 5 | Results from a permutation-based control analysis testing the effect of feature dimensionality on predictive modeling performance.** A grid search was conducted across feature sets of increasing size using randomly permuted connections. These feature sets were used to train an elastic net model to predict  $g$  scores on a held-out test sample using 5-fold cross-validation. Two-sided  $t$ -tests were used to examine whether performance metrics significantly related to feature

set size. **a** Performance as measured by Pearson correlation ( $r$ ) showed no relationship with feature set size ( $r = -0.081$  [ $-0.232, 0.075$ ];  $t(159) = -1.021$ ;  $p = 0.309$ ). **b** Performance as measured by coefficient of determination ( $R^2$ ) showed a negative relationship with feature set size ( $r = -0.724$  [ $-0.790, -0.641$ ];  $t(159) = -13.220$ ;  $p < 0.0001^{***}$ ).

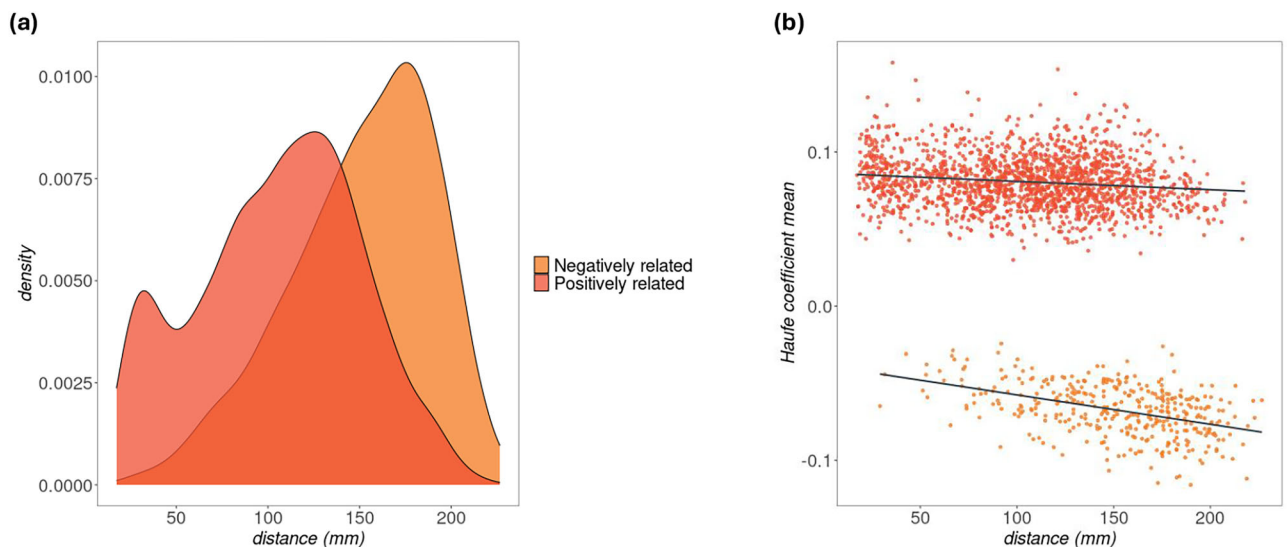


**Fig. 6 | Assessment of weak ties within the set of predictive connections.** **a** Comparison of distributions from connections negatively (orange) and positively (red) related to  $g$  using density estimation graphs with a Gaussian kernel and a Wilcoxon rank sum test. Distributions significantly differed from each other ( $W = 520005$ ;  $p < 0.0001$ ). **b** Scatter plot of the mean Haufe coefficient for each predictive connection against its distance, grouped by the direction of their association with  $g$ . The more a Haufe coefficient deviates from zero in either direction,

the more important its associated connection is for  $g$ . Two-sided  $t$ -tests were carried out to independently examine the correlation between the grouped Haufe coefficients and connection distance. Negative Haufe coefficients were negatively related to connection distance ( $r = -0.449$  [ $-0.527, -0.364$ ];  $t(371) = -9.683$ ;  $p < 0.0001^{***}$ ), and positive Haufe coefficients were also negatively related to connection distance ( $r = -0.145$  [ $-0.190, -0.099$ ];  $t(1786) = -6.179$ ;  $p < 0.0001^{***}$ ).

human connectome. We investigated the network architecture of intelligence, examining core predictions of NNT. Our investigation provided evidence that  $g$ : (1) engages multiple brain networks, supporting the theory's principle of distributed processing; (2) relies on weak, long-range connections, reflecting the theory's emphasis on a globally coordinated network architecture; (3) recruits regions that

orchestrate between-network interactions, supporting the predicted role of modal control mechanisms that drive global activity; and (4) depends on a small-world topology, the predicted architecture for system-wide communication and dynamics. Data from the Human Connectome Project<sup>30</sup> (HCP) demonstrated these patterns, in addition to data from the INSIGHT study<sup>5,31,32</sup> reported in the Supplemental

**Table 1 | Results from a multiple regression model predicting Haufe coefficients from the distance of predictive connections, their association with  $g$  (binarization code: positively related = 0, and negatively related = 1), and the interaction between these independent variables**

	Beta	SE	t	p
Distance	-5.38E-05	8.57E-06	-6.27	<0.0001***
Association	-1.25E-01	3.46E-03	-36.05	<0.0001***
Distance*Association	-1.37E-04	2.29E-05	-5.98	<0.0001***

Haufe coefficients that deviate from zero in either direction indicate greater importance for  $g$ . The sign merely indicates when weaker or stronger connections are found in higher  $g$  individuals (e.g., negative = weaker in higher  $g$ ; positive = stronger in higher  $g$ ). Two-sided  $t$ -tests were used to test the significance of beta coefficients.  $df = 829$ .

Materials (see Supplementary Figs. 1–14 and Supplemental Table 1). The reported findings, observed in a population of 976 participants, further establish and validate the predictions of the NNT framework and align with emerging evidence in network neuroscience, as we review in the following sections.

Prevailing theories of intelligence (see ref. 3 for an example) were formulated before the advent of network neuroscience and relied on brain imaging methods that were limited in their ability to capture global topological properties. For example, the classic P-FIT model was developed from a review of human neuroimaging studies aimed at identifying specific brain regions supporting complex problem solving<sup>33,34</sup>. However, how these regions communicated with one another to support higher cognition remained unclear. More recent research has acknowledged this limitation, emphasizing that structural connections play a critical role in shaping the brain's global functional topology<sup>11,18,27,28,35</sup>. Yet the few existing studies that have examined white-matter pathways associated with intelligence have relied on modeling techniques that are known to overlook weak, long-range connections, particularly those spanning multiple fiber bundles<sup>26</sup>. Thus, prior research has been largely insensitive to features that the NNT posits as central to the brain's global information processing architecture<sup>4</sup>. As a consequence of this limitation, prevailing theories of intelligence have continued to emphasize the central role of specific brain networks (e.g., the fronto-parietal network in the P-FIT model)<sup>3</sup>. To address this gap and more comprehensively characterize the neural foundations of intelligence, we employed a joint structure-function modeling approach that more accurately captures the global topology of the human connectome.

In our analysis, we recognized potential concerns about overfitting in the univariate feature selection step of a CPM framework<sup>36</sup>. To mitigate this issue and improve the generalizability of our results, we implemented an elastic net model within a stratified 5-fold cross-validation framework. The elastic net imposes regularization to prevent overfitting, while 5-fold cross-validation ensures training samples do not significantly overlap to increase generalizability. The large sample size of the HCP dataset ( $N = 831$ ) further strengthens the reliability and reproducibility of our predictive findings.

Our main connectome-based predictive model, which integrated structure-function connections across the whole-brain, accounted for a significant proportion of variance in  $g$  (12% in the HCP sample, and 15% in the INSIGHT study; Fig. 1a). These findings illustrate the contribution of the whole-brain connectome to individual differences in intelligence and align with recent studies in network neuroscience<sup>5–7</sup>. Notably, our HCP whole-brain model outperformed a recent study that predicted intelligence scores in held-out HCP participants from resting-state and diffusion-weighted data analyzed with structure-function coupling methods<sup>37</sup> (12% versus 6%). Moreover, our HCP whole-brain model similarly outperformed another coupling model applied to the HCP dataset that incorporated task-based functional

images rather than focusing solely on resting-state data<sup>38</sup> (12% versus <1–7%). These comparisons highlight the importance of jointly modeling structural and functional connectivity to capture their integrated contribution to brain organization, rather than relying on structure-function coupling approaches that quantify coherence without modeling their mutual influence. The benefits of a joint structure-function modeling framework are exemplified by its capacity to recover weak, long-range connections and to functionally constrain estimates of information flow bandwidth along structural pathways that diffusion-based tractography can only hypothesize.

Several other effective network modeling approaches have been developed to jointly model structural and functional information. For example, one framework maps higher-order relationships between structural and functional networks<sup>39</sup>, enabling the recovery of missing or underestimated edges, elucidating inter-network relationships, and capturing the topology of the high-dimensional space in which individual nodes are embedded. Other methods seek to improve the estimation of intrinsic connectivity networks (ICNs) through multi-modal independent component analyses<sup>40,41</sup>. These methods can produce multi-modal, data-driven parcellation schemes, link structural and functional connectivity information, enhance structure-function coupling between ICNs, and refine network boundaries. Collectively, these approaches offer a more comprehensive assessment of how structure-function relationships support high-level cognition<sup>42</sup>.

To investigate the NNT prediction that intelligence engages multiple brain networks, we examined the relative contributions of separate ICNs to the prediction of  $g$  scores. Rather than engaging a single network,  $g$  was associated with individual differences in a wide range of networks centered around cognitive control (FPN, CON), attention (DMN, DAN), language (LAN), and perceptual (V1, V2, AUD) processes. Prior research has emphasized the involvement of networks that support each of these functions in general intelligence<sup>43–46</sup>. However, despite their individual predictive power, exclusion analyses demonstrated that none of the networks are crucial for predicting individual differences in  $g$  within a whole-brain context. Between-network links appear in large part to drive this pattern, as demonstrated by the visualization of predictive connections (Fig. 4). Between-network connections with predictive power included network interactions involving all twelve ICNs, including those whose within-network connections were not predictive (OA, PMM, VMM), thereby supporting the NNT's principle of distributed processing for general intelligence (for converging evidence, see refs. 5–7, 47, 48). Together, these findings align with the NNT framework and necessitate a shift in perspective from a localizationist perspective to examining the emergence of  $g$  from system-wide network communication and dynamics.

According to the NNT framework, intelligence depends on the engagement of weak, long-range connections (i.e., weak ties) that enable efficient system-wide communication and dynamics<sup>9,11</sup>. These connections are hypothesized to allow the flexible reconfiguration of brain networks in response to changing task demands<sup>11–13</sup>. To investigate the role of weak ties in  $g$ , we examined how a connection's importance for  $g$  varied as a function of its length and strength. The joint structure-function model and the tractography method we employed provide distinct advantages in detecting weak, long-range connections compared with traditional approaches<sup>8,49</sup>.

Our findings revealed that, in individuals with higher  $g$ , weaker connections tended to span longer distances than stronger connections in the same individuals (Fig. 6a). Furthermore, the importance of weak connections for  $g$  increased with connection length, whereas the relevance of strong connections increased with shorter distances. In other words, among weak ties, those extending over longer distances were more strongly associated with  $g$ , while among strong ties, those spanning shorter distances were more closely linked to  $g$  (Fig. 6b). These findings align with prior research investigating measures of

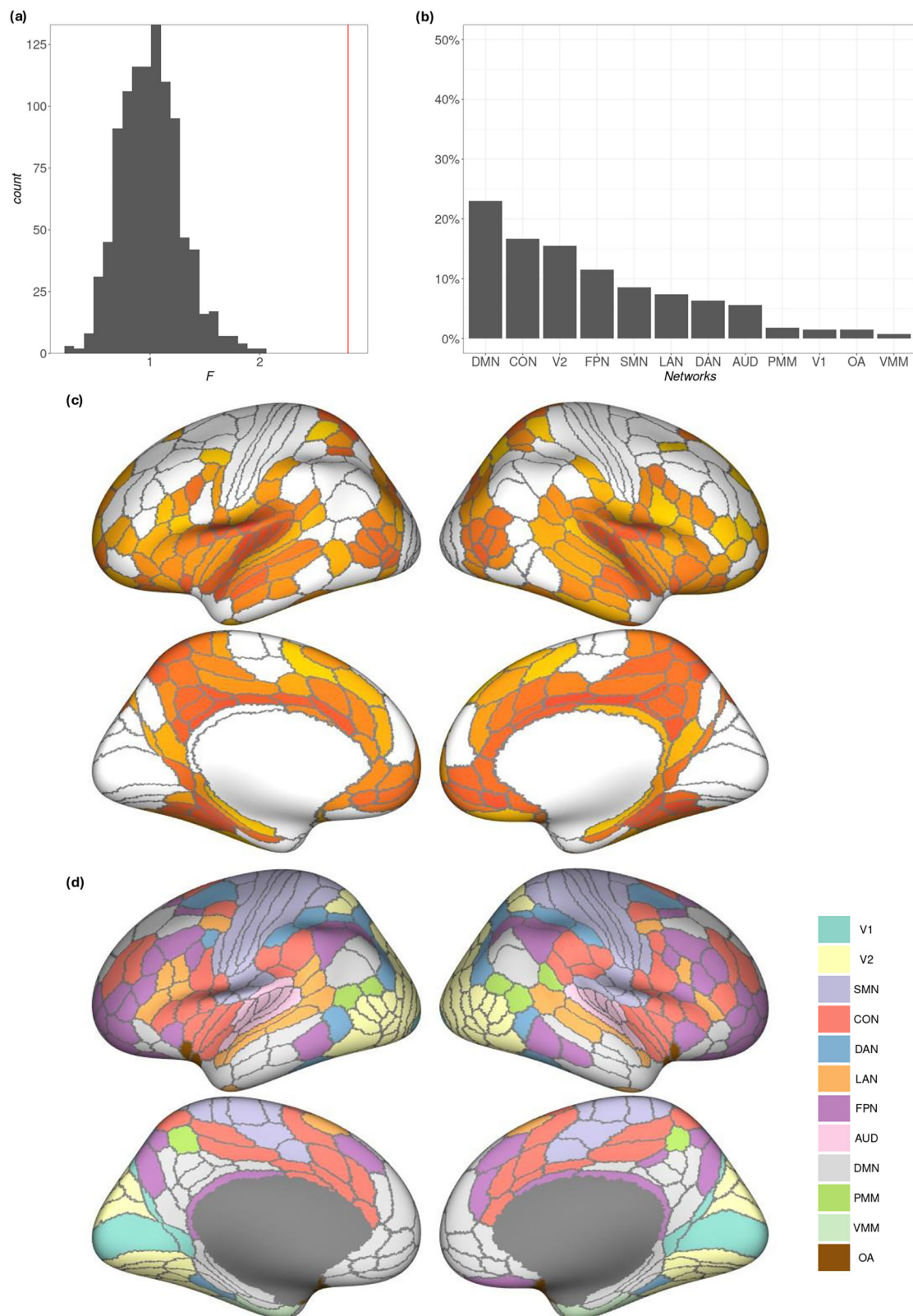


**Fig. 7 | Assessment of the relationship between  $g$  scores and cortical modal control profiles calculated from regions in after excluding the bottom 25th percentile. **a** Empirically derived null distribution of  $F$ -statistics from permutation testing with 1000 randomly shuffled distance matrices. The red line represents the statistical value from the MDMR model. **b** Bar graph displaying the percentage of the top 75th percentile regions coming from a given ICN. **c** Modal control value of regions in the top 75th percentile averaged across participants, by region, and plotted on the cortical surface. Lower values are closer to yellow, while higher**

values are closer to red. **d** Network assignments of regions plotted on the cortical surface. The color palette is consistent with Fig. 4. V1 Primary Visual Network, V2 Secondary Visual Network, SMN Somatomotor Network, CON Cingulo-opercular Network, DAN Dorsal Attention Network, LAN Language Network, FPN Frontoparietal Network, AUD Auditory Network, DMN Default Mode Network, PMM Posterior Multi-modal Network, VMM Ventral Multi-modal Network, OA Orbito-affective Network.

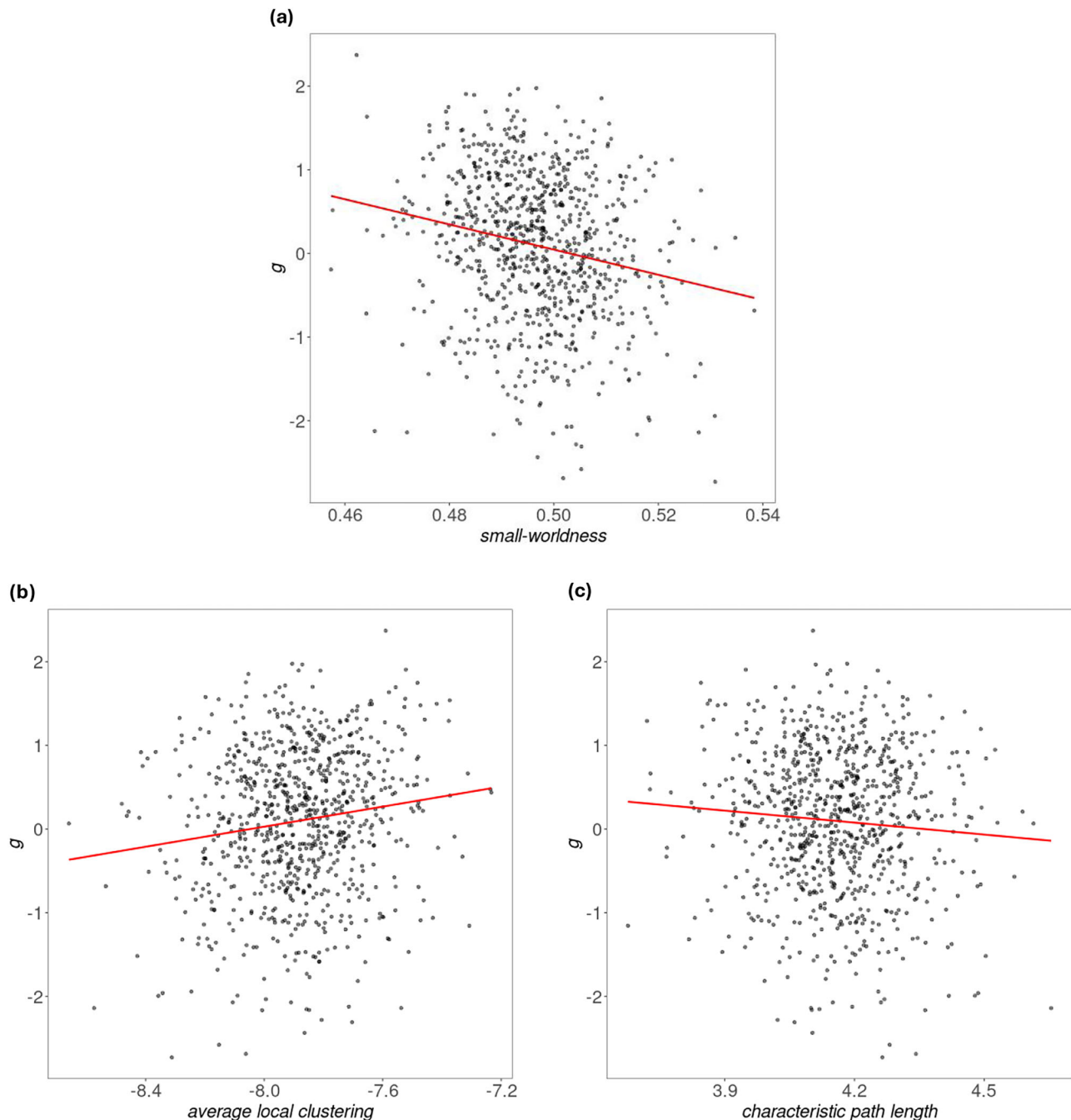


**Fig. 8 | Correlation models assessing the relationship between small-worldness, its underlying topological properties (i.e., local clustering and path length), and  $g$ .** Two-sided  $t$ -tests were carried out to assess the statistical significance of each Pearson correlation value. **a** Scatter plot of  $g$  scores against small-world propensity values showing a negative correlation ( $r = 0.204$  [−0.268, −0.137];  $t(829) = -5.986$ ;  $p < 0.0001^{***}$ ). Values deviating towards zero denote a more small-world, rather than random, network architecture. **b** Scatter plot of  $g$

scores against average local clustering (log transformed) showing a positive correlation ( $r = 0.143$  [0.076, 0.209];  $t(829) = 4.174$ ;  $p = 0.0004^{***}$ ). Higher values denote greater clustering. **c** Scatter plot of  $g$  scores against characteristic path length (i.e., shortest average path length) showing a negative correlation ( $r = -0.079$  [−0.146, −0.012];  $t(829) = -2.274$ ;  $p = 0.023^*$ ). Lower values denote shorter average path lengths.  $P$ -values were corrected for multiple comparisons using the false discovery rate.

functional connectivity, where weak functional associations were found to predict general<sup>10</sup> and fluid intelligence<sup>7,12</sup>. Our results contribute to this prior work by providing structural evidence, demonstrating that the physical length of direct connections between spatially distributed regions plays a critical role in supporting general intelligence. Furthermore, our findings motivate new insights into how connection strength and length interact to support  $g$ . Specifically, a topology characterized by shorter, stronger connections coupled with

longer, weaker connections appears to be conducive to higher cognitive functioning. This pattern of results supports the notion that a globally organized, economically efficient information processing architecture, proposed by the NNT framework, is crucial for intelligence.

A central question in the study of human intelligence concerns the nature of the top-down mechanisms that govern the selection and control of representations underlying goal-directed behavior. The

NNT framework proposes that brain network dynamics are shaped by the topology of the human connectome. That is, where specific brain regions are located, and where they can act as network controllers to effectively drive the system into specific functional states<sup>16,18</sup>. The hierarchical community structure of the brain may facilitate or constrain the transition from one state to another. Regions exhibiting greater modal control can drive the system towards difficult-to-reach states by using their connections to enable a sequence of less frequently engaged state transitions. Such transitions reflect the capacity to respond flexibly to novel situations by engaging mechanisms that support adaptive, goal-directed behavior<sup>18,19</sup>. Certain primary (e.g., SMN and AUD) and higher order ICNs (e.g., CON and FPN) are known to support adaptive responding through the control of mental operations, and are therefore expected to show higher modal control scores<sup>16</sup>. According to NNT, the efficiency of system-wide network function depends on modal control regions that orchestrate global network communication, suggesting that individual differences in these properties should predict  $g$ .

We found that participants' modal control profiles significantly predicted  $g$  (Fig. 7a), supporting the NNT framework. The profiles associated with  $g$  most prominently involved regions within the DMN, CON, FPN, and V2 networks, each of which also demonstrated high modal control values (Fig. 7b, c). Prior cortical mapping studies have shown that the CON, FPN, and V2 demonstrate high modal control values (see Fig. 2c in ref. 16). Beyond these networks, and consistent with prior research (Fig. 2c in ref. 16), the AUD and OA exhibited high modal control values (Fig. 7c). Collectively, our findings align with prior work indicating that hubs of modal controllability predominantly reside within cognitive control and primary sensory networks<sup>16</sup>.

Further, while modal control is not strictly a graph theoretic property, at least not in the same way local clustering or characteristic path length are, it does correlate highly with graph theoretic properties, namely weighted degree<sup>16</sup>. This suggests that certain topological properties may be driving factors in the creation and maintenance of structural control mechanisms. Thus, together with our findings, the prediction of general intelligence may also be informed by examining sparsely connected brain regions. Future research investigating this relationship may provide a complementary perspective on the relationship between modal control and  $g$ . In addition, other structural control mechanisms may also provide complementary insights, specifically average and boundary controllability. Within Network Control Theory, average controllability is hypothesized to enable easy-to-reach states<sup>16</sup>, which may reflect access to general knowledge structures<sup>4</sup>, and boundary controllability is hypothesized to enable states reflecting network integration<sup>16</sup>.

Consistent with NNT, prior neural communication models emphasize the importance of structural attributes in propagating functional signals between cortical regions, thereby shaping communication patterns that underlie high-level cognition<sup>27,28,35</sup>. These models often focus on topological properties, such as pathways through graph networks, that constrain the flow of information. The joint structure-function model adopted here incorporates similar constraints<sup>8</sup>. However, according to NNT, modal control adds further insight by demonstrating how structure not only constrains but also drives functional activation patterns, providing evidence that intelligence depends on regions that flexibly orchestrate global network activity.

According to NNT, a small-world topology is essential for the network architecture of intelligence, as it simultaneously ensures local and global efficiency. Network segregation, characterized by densely connected local modules, enhances local efficiency, while network integration, mediated by long-range connections, facilitates efficient global communication. The balance between these opposing principles (minimizing wiring costs versus maximizing global efficiency) allows for rapid functional reconfiguration and optimal performance

under changing task demands. While previous studies have primarily examined network integration<sup>24</sup> or segregation<sup>25</sup>, the present study investigates whether the balance between these two properties, captured by small-worldness, constitutes a critical organizational principle underlying general intelligence.

Consistent with NNT's prediction, we found that individuals with higher  $g$  scores exhibited global topologies more closely resembling a small-world architecture compared to those with lower  $g$  scores (Fig. 8a). Further analyses revealed that this relationship was driven by both greater local clustering (Fig. 8b) and shorter global path length (Fig. 8c). Previous studies have independently reported shorter path length<sup>24,50</sup> and greater local clustering in the functional topology in intelligence<sup>50</sup>. However, our findings demonstrate that the balance between these two properties, captured by small-worldness, predicts higher  $g$  scores, providing a framework for understanding the contributions of each topological attribute<sup>31</sup> to general intelligence.

Our analysis also clarified the kinds of deviations from a small-world topology that predict lower  $g$  scores. Specifically, we investigated whether individuals with lower  $g$  scores deviate towards more (1) random networks, associated with short path lengths but low local clustering, or (2) regular networks, associated with high local clustering but long path lengths. We found that individuals with lower  $g$  scores exhibit more randomness than regularity in their network organizations, suggesting a breakdown in local clustering (Fig. 8b). Yet, how do individuals with lower  $g$  scores exhibit deviations towards more random global topologies, as indicated by the small-world metric, given that more random network structures typically reduce path lengths? The answer may lie in optimal (i.e., less random) between-network connections that reduce global path lengths<sup>52</sup>. Thus, higher  $g$  individuals may achieve shorter path lengths through optimal placement of their neural connections rather than relying on more random placements.

In summary, Network neuroscience bridges the gap between traditional, localist approaches to brain function and globalist perspectives by leveraging network science to create a unified framework. Rather than dismissing localist findings, it explains how local features form essential building blocks within larger systems, where the mechanisms governing their interactions play a pivotal role in human cognition. This framework offers a common language and methodology to analyze brain topologies across all scales, encompassing molecules, synapses, networks, circuits, and entire systems.

Building on this progress, the Network Neuroscience Theory<sup>4</sup> of intelligence proposes that  $g$  arises from the brain's global organization. Our findings from the HCP dataset directly support this prediction. We observed that intelligence depends on a global architecture, with joint modeling of structural connections with intrinsic functional co-activation patterns across the whole brain explaining 12% of the variance in  $g$ . No single ICN matched this predictive power. Our findings validate the predictions of NNT, demonstrating that intelligence: (1) engages multiple networks; (2) relies on weak, long-range connections; (3) employs regions high in modal controllability that can drive global activity; and (4) depends on a small-world topology that simultaneously ensures local and global processing efficiency. In addition, we present analyses from an independent dataset that further support these predictions in the Supplemental Materials. Thus, our research provides empirical evidence to support core principles of NNT across multiple datasets and methodologies.

In conclusion, NNT offers a powerful, unifying theory to integrate findings from the general intelligence literature, acknowledging the importance of specific regions and networks that have been the focus of prior research while also paving the way for future explorations of the global topology and dynamics of the human connectome. Central questions that drive future research include: (1) how intelligence is constructed from the interaction(s) between multiple brain networks,

(2) how weak connections influence information flow, and (3) how specific control regions orchestrate global network communication. By addressing these questions, future research will achieve a deeper understanding of the nature of  $g$ , uncovering its origins within the global topology and dynamics of the human connectome.

We recognize several limitations in our analysis that motivate future research and advances in network neuroscience. First, although CPM is a well-validated predictive modeling framework, it is not the only approach taken in network neuroscience to elucidate the neurobiology of intelligence. We applied this linear modeling approach because it is well-suited to explain the macroscopic dynamics of resting-state networks<sup>53</sup>. Artificial neural network alternatives may help identify non-linear relationships for more accurate predictions of intelligence<sup>54</sup>. Second, convergent evidence from other multi-modal modeling techniques would enhance the generalizability of our findings. However, such alternatives must be designed in a way that captures local and global topological attributes of nodes in a system<sup>39,42</sup>. Third, while modal control is not strictly a graph theoretic property (e.g., local clustering, characteristic path length, etc.), it does correlate highly with graph theoretic properties, namely weighted degree. Given our findings, this suggests that the prediction of general intelligence may also be informed by examining sparsely connected brain regions. Future research examining this relationship may provide a complementary perspective on the matter.

## Methods

### Dataset

We obtained participant data ( $N=1206$ ) from the publicly available 1200-subject, young adult release of the Human Connectome Project<sup>30</sup> (HCP). Participants were aged 22–36 years ( $M=28.632$ ;  $SD=3.670$ ), and 54% were female. While our dataset was well balanced between males and females, our study focused on theoretical predictions with respect to all humans. Thus, an investigation into sex differences was deemed beyond the scope of this study, and no specific hypotheses were made. Informed consent was obtained for all participants prior to study enrollment. The institutional review board of the University of Illinois, Urbana-Champaign, reviewed and approved this study. Finally, this dataset included comprehensive cognitive and neuropsychological tests, as well as magnetic resonance imaging (MRI) data.

The cognitive test battery was comprised of several measures from the NIH toolbox ([nihtoolbox.org](http://nihtoolbox.org)) including: (1) the Picture Vocabulary Test (PicVocab), an assessment of vocabulary; (2) the Picture Sequence Memory Test (PicSeq), an assessment of episodic memory; (3) the Flanker Inhibitory and Attention Test (Flanker), an assessment of executive function; (4) the Dimensional Change Card Sort Test (CardSort), an assessment of cognitive flexibility; (5) the Pattern Comparison Processing Speed Test (ProcSpeed), an assessment of processing speed; (6) the Oral Reading Recognition Test (ReadEng), an assessment of reading decoding skills and crystallized abilities; and (7) the List Sorting Working Memory Test (ListSort), an assessment of working memory. Other measures included<sup>55</sup>, but not belonging to the NIH toolbox, were: (1) the Penn Matrix Test (PMA-T24\_A\_CR), a measure of non-verbal reasoning; (2) the Variable Short Penn Line Orientation Test (VSPLIT\_TC), a measure of visuospatial processing; and (3) the Penn Word memory test (IWRD\_TOT), a measure of verbal episodic memory.

MRI data consisted of structural, resting-state functional, and diffusion-weighted scans. The acquisition parameters and the minimal preprocessing pipeline implemented by the HCP team for each modality are extensively described in their original publication<sup>56</sup>. Resting-state data [TR = 720 milliseconds (ms); TE = 33.1 ms; 2 millimeter (mm) isotropic resolution; multiband acceleration factor = 8] were comprised of four separate scans, acquired on two separate days. Two scans were acquired on each day using two separate phase-encoding directions (i.e., left-to-right, right-to-left). Each scan was 14 min and

24 s long, resulting in 1200 volumes per scan. Diffusion-weighted scans [TR = 5520 ms; TE = 89.5 ms; 1.25 mm isotropic resolution] were obtained using a multi-shell protocol [b = 1000, 2000, 3000 s/mm<sup>2</sup>; 90 directions/shell]. All data were downloaded in their minimally pre-processed format.

### Subset procedure

We included only those participants who had completed all neuropsychological testing ( $N=1188$ ). To exclude those with cognitive impairment, a score of 27 or higher on the Mini-Mental Status Exam was required ( $N=1155$ ). We did not implement any data imputation. Therefore, participants with missing cognitive data were excluded ( $N=1151$ ). This subset of participants was used for modeling a latent  $g$  factor.

A subset of the subjects used for factor analysis had completed all resting-state and diffusion-weighted MRI scans ( $N=896$ ). We further implemented a movement threshold such that participants with a mean relative root-mean-squared movement parameter, as calculated by the HCP team (Movement\_RelativeRMS\_mean.txt), above 0.20 mm for any resting-state scan were excluded ( $N=866$ ). Finally, to ensure the quality of the final connectomes, we calculated their level of sparsity (i.e., the number of zeroes in the matrix). Connectomes comprised of an abnormally large number of zeroes were most likely generated from poor quality diffusion-weighted data. Thus, sparsity values were z-scored, and participants with a z-score greater than 3.5 were dropped ( $N=831$ ). This subset of participants was used for the brain-behavior analyses.

### Factor analysis

We adopted a hierarchical approach from prior work to derive a latent  $g$  factor from the dataset<sup>6</sup>. Here, a bi-factor model estimated a common factor,  $g$ , that loads onto all tests, and several group factors that load onto subsets of tests. This was done by running an exploratory factor analysis to extract first-order group factors from manifest-level variables and a second-order general factor from the first-order group factors. Then, an oblique rotation with a Schmid–Leiman transformation<sup>57</sup> was used to generate a bi-factor model where all manifest-level variables load onto all orthogonalized latent factors (i.e., general and group). Horn's parallel analysis was used to determine the number of latent factors underlying the data to be used in the exploratory analysis. This process compared eigenvalues (representing the amount of variance captured by a latent factor) derived from the observed data to those derived from random datasets of the same size. Factors with eigenvalues more than their random counterparts were retained.

While the bi-factor model guarantees that general and group factors will be extracted, the factor loadings, number of group factors, and fit of the model are ultimately determined by the data's structure. If a hierarchical structure truly exists in the data, then the model will produce good indices of fit. We report two types of these indices, including the comparative fit index (CFI) and root mean squared error approximation (RMSEA).

### Resting-state independent component analysis and spatial component classification

Resting-state images were smoothed using a 4 mm full-width-half-maximum (FWHM) kernel at 75% brightness threshold using FSL's *susan*. Smoothed images were then high-pass filtered at 0.01 Hz and linearly detrended using AFNI's *3dTproject*. FSL's *melodic-ica* was then applied to extract spatial co-activation patterns representative of signal (i.e., blood-oxygen-level-dependent neuronal activity) and noise (i.e., physiological artifacts). These spatial patterns were thresholded using probability maps supplied by the *melodic-ica* mixture model output. Voxels with less than a 50% probability of contributing to a spatial component were zeroed out.

We used a component classification approach similar to the automatic-removal-of-motion-artifacts method<sup>58</sup> (AROMA). First, the frequency content of spatial components was calculated from the Fourier-transformed mixture matrix supplied by the *melodic-ica* output. Components with a large amount of high-frequency content were discarded. Second, spatial components were robustly correlated with resting-state motion parameters. Components with a moderate correlation with in-scanner motion were discarded. Third, a Pearson's skewness index was calculated from the distribution of activation values for each component. Noise components are assumed to exhibit a zero-mean Gaussian distribution<sup>59</sup>. Thus, components with a Pearson's skewness index close to 0 were discarded. Finally, spatial components whose contributing voxels were not substantially within the grey matter were discarded.

Spatial components classified as signal were masked with the Glasser-360 parcellation. The total voxel-wise activation value for each cortical region within each spatial component was calculated. These values were then stacked into an activation matrix, such that columns represented spatial components, rows represented cortical regions of interest, and values described the total activation of a cortical region for that spatial component. Matrices were then normalized to a range between 0 and 1. These matrices served as the functional input for the joint structure-function network model.

### Diffusion-weighted tractography

We adopted multi-shell, multi-tissue, constrained spherical deconvolution (MSMT-CSD)<sup>49</sup>, a state-of-the-art tractography algorithm to model the brain's white matter pathways. This method works to produce a high-quality estimation of a fiber orientation distribution function (FODF) for each voxel in the brain. These functions describe the likelihood and strength of water flow in each direction within a voxel. The values are used by probabilistic tractography algorithms to trace white-matter pathways (i.e., streamlines). Importantly, MSMT-CSD can capture multiple directions of water flow in a single voxel, making it an ideal approach to accurately model white matter pathways in cross-fiber areas. All functions used for diffusion-weighted tractography were implemented by the *mrtrix3* software<sup>60</sup>.

To prepare for MSMT-CSD tractography, preprocessed diffusion-weighted images were bias-corrected with the *dwibiascorrect* function. Multi-tissue response functions were calculated from bias-corrected images with the *dwi2response* function and the *dhollander* algorithm. Response functions were then averaged across all subjects. The group-averaged response functions were used to estimate FODFs with the *dwi2fodf* function. FODFs were then normalized using the *mtnormalise* function. Tractography was run using the *tckgen* function with the iFOD2 algorithm, a selection of 50 million streamlines, a FODF amplitude cutoff of 0.06, a minimum tract length of 5 mm, a maximum tract length of 275 mm, a step size of 1.25 mm, and an angle cutoff of 45°.

We processed the resulting tractograms with the second iteration of the Spherical-deconvolution Informed Filtering of Tractograms<sup>61</sup> (SIFT2) algorithm. This method addresses the streamline connectivity quantification problem<sup>62</sup> by generating a more biologically relevant measure of white-matter connectivity strength. Intuitively, connectivity strength can be conceptualized as the number of axons making up a fiber bundle (i.e., its density). The denser a fiber bundle is, the greater its information-carrying capacity. Because diffusion-weighted imaging cannot capture individual axons, the strength of water diffusion is used as a proxy and modeled with FODFs. While this information is used in tractography algorithms to trace pathways, it is not routinely integrated into a measure of connectivity strength. Instead, traditional structural connectomes simply reflect the total number of streamlines (i.e., pathway traces) between cortical regions. This does not capture connectivity strength in a quantitative sense, as streamlines are akin to lines on a page with no real associated volume.

The SIFT2 algorithm works to combine streamlines with their associated density information to generate a metric that more accurately reflects information-carrying capacity, referred to as fiber bundle capacity (see ref. 62 for an in-depth discussion). Finally, we applied the Glasser-360 parcellation to these filtered tractograms to obtain a structural connectome. These served as the structural input for the joint structure-function model.

### Joint structure-function network modeling

The joint structure-function model takes two primary inputs: (1) a functional activation matrix ( $R_i^m$ ) whose values describe the functional activation of each region,  $i$ , contributing to some functional co-activation pattern,  $m$ ; and (2) a structural connectome ( $D_l$ ) whose values describe the white-matter connectivity strength,  $l$ , between all pairs of cortical regions. These inputs are used to estimate two unknowns, the flow and the capacity adjustment variables.

The flow variable ( $f_l^m$ ) extracts function-related, structural brain circuits that describe the capacity of a structural edge,  $l$ , to transmit functional information in support of a functional co-activation pattern,  $m$ . This is termed information flow capacity. This is related to the fiber bundle capacity measure within the structural connectomes in terms of bandwidth (i.e., the capacity of a connection to transfer information). However, it differs in that it is functionally informed, rather than a purely structural estimate that can only be hypothesized to align with a given functional bandwidth. The capacity adjustment variable ( $P_l$ ) works to ensure a node's anatomical connections are sufficiently strong for supporting an observed functional pattern by allowing the model to correct for underestimated white-matter pathways.

In solving for  $f_l^m$  and  $P_l$ , several constraints are established to integrate structural and functional information, while a cost function is defined to determine the optimal solution. The first constraint is known as the link capacity constraint (Eq. 1). This constraint puts an upper bound on the amount of information a given link,  $l$ , can transmit in the service of all functional patterns ( $m \in M$ ):

$$\sum_{m=1}^M f_l^m \leq (D_l + P_l), \forall l = 1, 2, \dots, L. \quad (1)$$

The second constraint is known as the node demand constraint (Eq. 2). This constraint ensures that the amount of information being delivered to a given node by its links ( $l \in N_i$ ) is sufficient to support its observed functional activation across all functional modes ( $r \in R_i$ ):

$$\sum_{l \in N(i)} f_l^m \geq r_i^m, \forall m = 1, 2, \dots, M, i = 1, 2, \dots, N. \quad (2)$$

These two constraints establish the integrative framework for structural and functional connectivity that applies to the flow variable. The third constraint is known as the feasibility constraint (Eq. 3). This constraint ensures that information carried between two regions,  $i$  and  $j$ , cannot arbitrarily exceed the amount of information flow necessary to support their observed neuronal activities:

$$f_l^m \leq \max\{R_i^m, R_j^m\} \text{ where } l = (i, j), \forall l = 1, 2, \dots, L. \quad (3)$$

Finally, the cost function (Eq. 4) works to minimize the information delivery cost while enhancing underestimated structural connections, if necessary, to ensure anatomical pathways can feasibly support observed functional co-activation patterns:

$$C(f_l^m, P_l) = \sum_{l=1}^L \left( \frac{1}{D_l} \sum_{m=1}^M f_l^m \right) + \rho \sum_{l=1}^L \left[ \left( 1 + \frac{1}{D_l} \right) P_l \right] \quad (4)$$

Where  $\rho$  is a hyperparameter with the default value of 0.02 as set by Chu and colleagues<sup>8</sup>. The overall network optimization problem is

summarized as:

$$\min_{f_l^m \geq 0, P_l \geq 0} \sum_{l=1}^L \left( \frac{1}{D_l} \sum_{m=1}^M f_l^m \right) + \rho \sum_{l=1}^L \left[ \left( 1 + \frac{1}{D_l} \right) P_l \right]$$

The solution is derived subject to constraints 1, 2, and 3 using standard optimization techniques. This results in  $m \times N \times N$  multi-modal connectomes, where  $m$  is the number of co-activation patterns recovered by the ICA, and  $N$  is the number of cortical regions indicated by the adopted parcellation scheme (Glasser-360). Each  $m_i$  connectome represents a single function-informed, structural brain circuit. Values represent the capacity of a connection within this circuit to transmit functional information in association with some intrinsic functional co-activation pattern. Given the integrated nature of the brain's intrinsic connectivity networks<sup>63,64</sup> (ICNs), each brain circuit contains both within- and between-network connections. Here, we define ICNs using the Cole-Anticevic Brain-wide Network Partition<sup>65</sup> (CAB-NP) that was developed using the Human Connectome Project dataset.

### Connectome-based predictive modeling

We conducted a connectome-based predictive modeling (CPM) analysis with stratified 5-fold cross-validation to predict out-of-sample  $g$  scores from the structure-function brain circuits across the whole brain. Within each subject and session, for all connections in  $N_l$ , we extracted their set of counterparts across the  $m$  structure-function brain circuits. The maximum value within each connection's set was retained as empirical evidence for its observed information flow capacity. This allowed us to create one whole brain  $N \times N$  multi-modal connectome per session per participant. These were averaged across sessions within subjects and used in analyses. CPM using these final connectomes was conducted with the following steps: (1)  $g$  scores were binned into quartiles and randomly sampled equally from each quartile into 5 separate folds; (2) a training set was constructed from 4 folds, while the remaining fold made up the test set; (3) connectivity features were standardized (i.e., z-scored), correlated with  $g$  scores, and features with a  $p$ -value above 0.1 were discarded; (4) the remaining connections were used to fit an elastic net model from the training set using stratified 3-fold cross-validation; and (5) connectivity features in the test set were z-scored using parameters calculated from the training set and used to make predictions for the held-out test set. This process was then repeated until all 5 folds served as a test set.

We report multiple metrics to quantify the success of structure-function connections to predict test set  $g$  scores in the CPM framework. This includes a Pearson correlation coefficient ( $r$ ), a coefficient of determination ( $R^2$ ), and a normalized root mean square deviation ( $nRMSD$ ) between the observed and predicted  $g$  scores. We used the cross-validation formula to generate the coefficient of determination:

$$R^2 = 1 - \frac{\sum (y_{obs} - y_{pred})^2}{\sum (y_{obs} - y_{obs,train})^2}$$

Note that the observed mean comes from the training set and does not include observed values from the test set. Thus,  $R^2$  does not simply equal the correlation squared. This is important to account for, because prediction outliers can artificially inflate the observed vs. predicted correlation, thereby giving the impression that the model performed well. The coefficient of determination formula used here is robust to such outliers and provides a more accurate measure of model performance. For example,  $R^2$  values are typically negative when highly positive performance correlations are due solely to extreme outliers.

Finally, to assess the statistical significance of CPM results, we conducted a permutation test with 1000 random permutations, following established conventions<sup>66</sup>. This method creates a null distribution by randomly shuffling scores between subjects and running the predictive model in the same manner. Permutation testing is

necessary to establish statistical significance in cross-validation frameworks because folds are not statistically independent from one another, precluding the use of standard parametric tests. Further, the use of regularization and a 5-fold cross-validation scheme results in much less training set overlap, is less biased compared to a leave-one-out scheme, prevents overfitting, and confirms the generalizability of the test's findings.

### Lesion analysis

To assess the predictive power of each ICN compared to our whole-brain model, we adopted a lesion approach that predicts out-of-sample  $g$  scores from subsets of connectivity features. This consisted of inclusion and exclusion predictive models. Inclusion models incorporated features from only one of the ICNs at a time. This allowed us to test the independent predictive efficacy of each ICN compared to the whole-brain model. Conversely, exclusion models iteratively removed each ICN from the whole-brain model while keeping all other features intact. This allowed us to see whether any ICN is crucial for the accurate prediction of  $g$  scores in the whole-brain model. A common concern regarding the comparison of whole-brain models to more localized, ICN-specific models is that performance is biased by the feature set size. Prior research has investigated this potential source of bias by performing grid searches across sets of varying sizes comprised of randomly selected edges. These are then used to fit predictive models in the same fashion as the originally described cross-validation procedure. Results from these investigations have consistently shown that the greater predictive performance of whole-brain models compared to more localized models is not simply due to larger feature set sizes<sup>5,7</sup>. We examined this issue as well, conducting a permutation-based control analysis. Here, a grid search across feature sets of increasing size, each populated with randomly permuted connections, was used to fit CPMs within the previously described framework.

### Topological characterization of $g$

With respect to network topology, we examined whether weak ties (i.e., weak, long-range connections) were important for  $g$ . For these analyses, we retained only highly stable connections that survived the feature selection step described above across all five folds. Additionally, we examined whether modal control, a structural control mechanism that facilitates global, functional brain movement towards difficult-to-reach states<sup>16,17</sup>, significantly related to  $g$ .

**Assessment of weak ties.** To assess whether significant connections included weak ties, we examined whether connections weaker in bandwidth within higher  $g$  individuals, compared to lower  $g$  individuals, were longer than those that were stronger in higher  $g$  individuals. It is important to note that connectivity features were standardized (i.e., z-scored) before model fitting. Given this standardization, a negative association is the direction we would expect to find concerning weak ties. That is, features with negative beta coefficients (i.e., negatively related) indicate features whose weakness is important for  $g$  (i.e., weaker in higher  $g$  individuals compared to lower  $g$  individuals). Here, we constructed distributions of connection length, averaged across all participants, and grouped by their direction of outcome association (i.e., connections negatively or positively related to  $g$ ). Because these distributions are somewhat skewed, the non-parametric Wilcoxon ranked-sum test with continuity correction was used. The length of each connection, in millimeters, was determined by the previously described tractography approach.

Next, we examined whether the importance of connections for  $g$  changed as a function of connection length and direction of outcome association. Specifically, when examining weak ties, does their importance for  $g$  increase with their length? Here, feature importance is defined as the contribution a feature makes to the variance among connections that is structured in relation to  $g$ . While it may seem that

beta coefficients describe feature importance, they only describe how features are used to make predictions. Machine learning models that incorporate regularization methods can artificially reduce beta coefficients of important features to, or close to, zero due to multicollinearity, and to reduce overfitting. Thus, they do not accurately describe the relevance of a given feature for the outcome, but rather how they contribute to making predictions. To correct for this, the Haufe transformation multiplies the beta coefficient vector by the original covariance matrix, thereby reintroducing shared variance among features to the model weights. As such, covariance-weighted model parameters no longer reflect their use for making predictions, but rather reflect an interpretable relation with the outcome in terms of relevance (see ref. 67 for a detailed discussion). Here, each feature's Haufe coefficient was averaged across all 5 folds. A multiple regression model was then fit to predict Haufe coefficients from connection length moderated by direction of outcome association.

**Assessment of modal controllability.** To investigate whether  $g$  is related to the orchestration of global network activity, we calculated modal control metrics. Modal control is a structural control mechanism that reflects the ability of a cortical region to move the brain towards and between functional states underlying effortful cognition (i.e., difficult-to-reach states). As modal control is a purely structural mechanism, the metric was generated from structural connectomes (see refs. 16,17 for details). To remove regions particularly weak in modal control, we averaged modal control values across subjects by region and identified those in the bottom 25<sup>th</sup> percentile. These were subsequently removed from analyses.

We adopted multivariate distance-based matrix regression<sup>68</sup> (MDMR) to assess the relationship between modal control and  $g$ . MDMR is a useful non-parametric approach when analyzing the relationship between many variables, where multiple comparisons correction may be an issue, and/or the number of features to be analyzed exceeds the number of observations. Here, a distance matrix is created describing how similar/dissimilar participants are in some high-dimensional information space described by the features of interest. The results can be interpreted as individual differences in the participants' cortical modal control profiles. We used distance-correlation to calculate the matrices. The total variance in each matrix is partitioned into pieces explained by a predictor or predictors of interest (e.g.,  $g$ ). For significance testing, an  $F$ -statistic is generated. However, because MDMR uses a non-parametric, distance-based approach, it does not follow a normal  $F$ -distribution. Thus, a permutation test is carried out, where the rows and columns of the distance matrix are randomly shuffled, the model is fit again, and an  $F$ -statistic is extracted. This is repeated many times to generate an empirically derived null distribution that can be compared with the observed  $F$ -statistic. The associated  $p$ -value reflects the number of  $F$ -statistics that equal or exceed the observed  $F$ -statistic, divided by the total number of  $F$ -statistics.

### Small-world characterization of $g$

We investigated whether  $g$  relies on the brain's global, small-world topology. We employed Telesford and colleagues<sup>69</sup> improvements upon the approach proposed by Watts and Strogatz<sup>70,71</sup> to extract a measure of small-worldness. Values close to 0 indicate small-world topologies, values closer to -1 indicate a deviation towards a more locally integrated, globally segregated, regular network, and values closer to 1 indicate a deviation towards a more locally segregated, globally integrated, random network. To further examine the relationship between  $g$  and specific elements of a small-world topology, we also report average shortest path length (i.e., characteristic path length) and average local clustering. For clarity, the average shortest path length was calculated using the topology of the joint structure-

function connectomes. This metric reflects the average shortest number of connections that must be traversed between all pairwise nodes. The anatomical coordinates of cortical regions and their geometric distances were not used. In addition, average local clustering was calculated using the Onnela function. This metric reflects the average intensity of triangles around a node.<sup>72</sup> These relationships were examined using a correlation-based approach.

### Reporting summary

Further information on research design is available in the Nature Portfolio Reporting Summary linked to this article.

### Data availability

The data that support the main findings of this study are available from the Human Connectome Project [www.humanconnectome.org/study/hcp-young-adult](http://www.humanconnectome.org/study/hcp-young-adult). The data that support findings in the supplemental materials are not currently available to the public. This is due to the fact that the original informed consent protocol did not include provisions for data sharing, and therefore, ethical restrictions prevent the distribution of participant data. Data for all figures are available in the Source Data.zip file accompanying this manuscript. Source data are provided with this paper.

### Code availability

Code for data processing and analyses related to results presented in the main text are available at [www.github.com/ramseywilcox/jsfm\\_hcp](https://www.github.com/ramseywilcox/jsfm_hcp). Code for data processing and analyses related to results in the supplemental materials are available at [www.github.com/ramseywilcox/jsfm\\_insight](https://www.github.com/ramseywilcox/jsfm_insight).

### References

- Jensen, A. R. *The g Factor: The Science of Mental Ability*. (Praeger, Westport, 1998).
- Barbey, A. K., Colom, R. & Grafman, J. Dorsolateral prefrontal contributions to human intelligence. *Neuropsychologia* **51**, 1361–1369 (2013).
- Jung, R. E. & Haier, R. J. The parieto-frontal integration theory (P-FIT) of intelligence: converging neuroimaging evidence. *Behav. Brain Sci.* **30**, 135–154 (2007).
- Barbey, A. K. Network neuroscience theory of human intelligence. *Trends Cogn. Sci.* **22**, 8–20 (2018).
- Anderson, E. D. & Barbey, A. K. Investigating cognitive neuroscience theories of human intelligence: a connectome-based predictive modeling approach. *Hum. Brain Mapp.* **44**, 1647–1665 (2023).
- Dubois, J., Galdi, P., Paul, L. K. & Adolphs, R. A distributed brain network predicts general intelligence from resting-state human neuroimaging data. *Philos. Trans. R. Soc. B Biol. Sci.* **373**, 20170284 (2018).
- Wilcox, R. R. & Barbey, A. K. Connectome-based predictive modeling of fluid intelligence: evidence for a global system of functionally integrated brain networks. *Cereb. Cortex* **33**, 10322–10331 (2023).
- Chu, S.-H., Parhi, K. K. & Lenglet, C. Function-specific and enhanced brain structural connectivity mapping via joint modeling of diffusion and functional MRI. *Sci. Rep.* **8**, 4741 (2018).
- Gallos, L. K., Makse, H. A. & Sigman, M. A small world of weak ties provides optimal global integration of self-similar modules in functional brain networks. *Proc. Natl. Acad. Sci. USA* **109**, 2825–2830 (2012).
- Santarnecchi, E., Galli, G., Polizzotto, N. R., Rossi, A. & Rossi, S. Efficiency of weak brain connections support general cognitive functioning. *Hum. Brain Mapp.* **35**, 4566–4582 (2014).
- Park, H.-J. & Friston, K. Structural and functional brain networks: from connections to cognition. *Science* **342**, 1238411 (2013).

12. Cole, M. W., Yarkoni, T., Repovš, G., Anticevic, A. & Braver, T. S. Global connectivity of prefrontal cortex predicts cognitive control and intelligence. *J. Neurosci.* **32**, 8988–8999 (2012).
13. Miller, E. K. & Cohen, J. D. An integrative theory of prefrontal cortex function. *Annu. Rev. Neurosci.* **24**, 167–202 (2001).
14. Cole, M. W. et al. Multi-task connectivity reveals flexible hubs for adaptive task control. *Nat. Neurosci.* **16**, 1348–1355 (2013).
15. Simon, J. D. & Mitter, S. K. A theory of modal control. *Inf. Control* **13**, 316–353 (1968).
16. Gu, S. et al. Controllability of structural brain networks. *Nat. Commun.* **6**, 8414 (2015).
17. Karrer, T. M. et al. A practical guide to methodological considerations in the controllability of structural brain networks. *J. Neural Eng.* **17**, 026031 (2020).
18. Betzel, R. F., Gu, S., Medaglia, J. D., Pasqualetti, F. & Bassett, D. S. Optimally controlling the human connectome: the role of network topology. *Sci. Rep.* **6**, 30770 (2016).
19. Beynel, L. et al. Structural controllability predicts functional patterns and brain stimulation benefits associated with working memory. *J. Neurosci.* **40**, 6770–6778 (2020).
20. Tang, R. et al. Longitudinal association of executive function and structural network controllability in the aging brain. *GeroScience* **45**, 837–849 (2023).
21. Bullmore, E. & Sporns, O. The economy of brain network organization. *Nat. Rev. Neurosci.* **13**, 336–349 (2012).
22. Bassett, D. S. & Bullmore, E. Small-world brain networks. *The Neuroscientist* **12**, 512–523 (2006).
23. Bassett, D. S. & Bullmore, E. T. Small-world brain networks revisited. *The Neuroscientist* **23**, 499–516 (2017).
24. Heuvel, M. P., van den, Stam, C. J., Kahn, R. S. & Pol, H. E. H. Efficiency of functional brain networks and intellectual performance. *J. Neurosci.* **29**, 7619–7624 (2009).
25. Hilger, K., Ekman, M., Fiebach, C. J. & Basten, U. Intelligence is associated with the modular structure of intrinsic brain networks. *Sci. Rep.* **7**, 16088 (2017).
26. Markov, N. T. et al. Weight consistency specifies regularities of macaque cortical networks. *Cereb. Cortex* **21**, 1254–1272 (2011).
27. Avena-Koenigsberger, A., Misisic, B. & Sporns, O. Communication dynamics in complex brain networks. *Nat. Rev. Neurosci.* **19**, 17–33 (2018).
28. Hermundstad, A. M. et al. Structural foundations of resting-state and task-based functional connectivity in the human brain. *Proc. Natl. Acad. Sci. USA* **110**, 6169–6174 (2013).
29. Hu, L. & Bontler, P. M. Cutoff criteria for fit indexes in covariance structure analysis: conventional criteria versus new alternatives. *Struct. Equ. Model. Multidiscip. J.* **6**, 1–55 (1999).
30. Van Essen, D. C. et al. The WU-Minn human connectome project: an overview. *NeuroImage* **80**, 62–79 (2013).
31. Zwilling, C. E. et al. Enhanced decision-making through multimodal training. *Npj Sci. Learn.* **4**, 11 (2019).
32. Daugherty, A. M. et al. Individual differences in the neurobiology of fluid intelligence predict responsiveness to training: evidence from a comprehensive cognitive, mindfulness meditation, and aerobic exercise intervention. *Trends Neurosci. Educ.* **18**, 100123 (2020).
33. Prabhakaran, V., Smith, J. A. L., Desmond, J. E., Glover, G. H. & Gabrieli, J. D. E. Neural substrates of fluid reasoning: an fMRI study of neocortical activation during performance of the raven's progressive matrices test. *Cognit. Psychol.* **33**, 43–63 (1997).
34. Kroger, J. K. et al. Recruitment of anterior dorsolateral prefrontal cortex in human reasoning: a parametric study of relational complexity. *Cereb. Cortex* **12**, 477–485 (2002).
35. Bassett, D. S., Zurn, P. & Gold, J. I. On the nature and use of models in network neuroscience. *Nat. Rev. Neurosci.* **19**, 566–578 (2018).
36. O'Connor, D., Lake, E. M. R., Scheinost, D. & Constable, R. T. Resample aggregating improves the generalizability of connectome predictive modeling. *NeuroImage* **236**, 118044 (2021).
37. Popp, J. L. et al. Structural-functional brain network coupling predicts human cognitive ability. *NeuroImage* **290**, 120563 (2024).
38. Popp, J. L. et al. Structural-functional brain network coupling during cognitive demand reveals intelligence-relevant communication strategies. *Commun. Biol.* **8**, 855 (2025).
39. Rosenthal, G. et al. Mapping higher-order relations between brain structure and function with embedded vector representations of connectomes. *Nat. Commun.* **9**, 2178 (2018).
40. Wu, L. & Calhoun, V. Joint connectivity matrix independent component analysis: auto-linking of structural and functional connectivities. *Hum. Brain Mapp.* **44**, 1533–1547 (2023).
41. Fouladivanda, M. et al. A spatially constrained independent component analysis jointly informed by structural and functional network connectivity. *Netw. Neurosci.* **8**, 1212–1242 (2024).
42. Levakov, G., Faskowitz, J., Avidan, G. & Sporns, O. Mapping individual differences across brain network structure to function and behavior with connectome embedding. *NeuroImage* **242**, 118469 (2021).
43. Braver, T. S. The variable nature of cognitive control: a dual mechanisms framework. *Trends Cogn. Sci.* **16**, 106–113 (2012).
44. Dohmatob, E., Dumas, G. & Bzdok, D. Dark control: the default mode network as a reinforcement learning agent. *Hum. Brain Mapp.* **41**, 3318–3341 (2020).
45. Colom, R., Karama, S., Jung, R. E. & Haier, R. J. Human intelligence and brain networks. *Dialogues Clin. Neurosci.* **12**, 489–501 (2010).
46. Melnick, M. D., Harrison, B. R., Park, S., Bennetto, L. & Tadin, D. A strong interactive link between sensory discriminations and intelligence. *Curr. Biol.* **23**, 1013–1017 (2013).
47. Dhamala, E., Jamison, K. W., Jaywant, A. & Kuceyeski, A. Shared functional connections within and between cortical networks predict cognitive abilities in adult males and females. *Hum. Brain Mapp.* **43**, 1087–1102 (2022).
48. Dhamala, E., Jamison, K. W., Jaywant, A., Dennis, S. & Kuceyeski, A. Distinct functional and structural connections predict crystallized and fluid cognition in healthy adults. *Hum. Brain Mapp.* **42**, 3102–3118 (2021).
49. Tournier, J.-D., Calamante, F. & Connelly, A. Robust determination of the fibre orientation distribution in diffusion MRI: non-negativity constrained super-resolved spherical deconvolution. *NeuroImage* **35**, 1459–1472 (2007).
50. Langer, N. et al. Functional brain network efficiency predicts intelligence. *Hum. Brain Mapp.* **33**, 1393–1406 (2012).
51. Kruschwitz, J. D., Waller, L., Daedelow, L. S., Walter, H. & Veer, I. M. General, crystallized and fluid intelligence are not associated with functional global network efficiency: a replication study with the human connectome project 1200 data set. *NeuroImage* **171**, 323–331 (2018).
52. Alizadeh Darbandi, S. S., Fornito, A. & Ghasemi, A. The impact of input node placement in the controllability of structural brain networks. *Sci. Rep.* **14**, 6902 (2024).
53. Nozari, E. et al. Macroscopic resting-state brain dynamics are best described by linear models. *Nat. Biomed. Eng.* **8**, 68–84 (2024).
54. Kulathunga, N. et al. Effects of nonlinearity and network architecture on the performance of supervised neural networks. *Algorithms* **14**, 51 (2021).
55. Moore, T. M., Reise, S. P., Gur, R. E., Hakonarson, H. & Gur, R. C. Psychometric properties of the Penn computerized neurocognitive battery. *Neuropsychology* **29**, 235–246 (2015).
56. Glasser, M. F. et al. The minimal preprocessing pipelines for the Human Connectome Project. *NeuroImage* **80**, 105–124 (2013).
57. Schmid, J. & Leiman, J. M. The development of hierarchical factor solutions. *Psychometrika* **22**, 53–61 (1957).

58. Pruim, R. H. R. et al. ICA-AROMA: a robust ICA-based strategy for removing motion artifacts from fMRI data. *NeuroImage* **112**, 267–277 (2015).
  59. Beckmann, C. F. & Smith, S. M. Probabilistic independent component analysis for functional magnetic resonance imaging. *IEEE Trans. Med. Imaging* **23**, 137–152 (2004).
  60. Tournier, J.-D. et al. *MRtrix3*: A fast, flexible and open software framework for medical image processing and visualisation. *NeuroImage* **202**, 116137 (2019).
  61. Smith, R. E., Tournier, J.-D., Calamante, F. & Connelly, A. SIFT2: enabling dense quantitative assessment of brain white matter connectivity using streamlines tractography. *NeuroImage* **119**, 338–351 (2015).
  62. Smith, R. E., Raffelt, D., Tournier, J.-D. & Connelly, A. Quantitative streamlines tractography: methods and inter-subject normalisation. *Aperture Neuro.* **2**, 1–25 (2022).
  63. Raichle, M. E. et al. A default mode of brain function. *Proc. Natl. Acad. Sci. USA* **98**, 676–682 (2001).
  64. Fox, M. D. & Raichle, M. E. Spontaneous fluctuations in brain activity observed with functional magnetic resonance imaging. *Nat. Rev. Neurosci.* **8**, 700–711 (2007).
  65. Ji, J. L. et al. Mapping the human brain's cortical-subcortical functional network organization. *NeuroImage* **185**, 35–57 (2019).
  66. Shen, X. et al. Using connectome-based predictive modeling to predict individual behavior from brain connectivity. *Nat. Protoc.* **12**, 506–518 (2017).
  67. Haufe, S. et al. On the interpretation of weight vectors of linear models in multivariate neuroimaging. *NeuroImage* **87**, 96–110 (2014).
  68. Anderson, M. J. A new method for non-parametric multivariate analysis of variance. *Austral. Ecol.* **26**, 32–46 (2001).
  69. Telesford, Q. K., Joyce, K. E., Hayasaka, S., Burdette, J. H. & Laurienti, P. J. The ubiquity of small-world networks. *Brain Connect* **1**, 367–375 (2011).
  70. Watts, D. J. & Strogatz, S. H. Collective dynamics of 'small-world' networks. *Nature* **393**, 440–442 (1998).
  71. Humphries, M. D. & Gurney, K. Network 'Small-World-Ness': a quantitative method for determining canonical network equivalence. *PLoS ONE* **3**, e0002051 (2008).
  72. Onnela, J.-P., Saramäki, J., Kertész, J. & Kaski, K. Intensity and coherence of motifs in weighted complex networks. *Phys. Rev. E* **71**, 065103 (2005).
- 2019-HR0011990067 to the University of Illinois at Urbana-Champaign (PI: Aron K. Barbey). The views and conclusions contained herein are those of the authors and should not be interpreted as necessarily representing the official policies or endorsements, either expressed or implied, of the IARPA, DARPA, or US Government.

### Author contributions

R.R.W.: data curation, formal analysis, methodology, software, validation, visualization, writing—original draft, writing—review and editing. B.H.: methodology, writing—original draft, writing—review and editing. L.L.V.: methodology, writing—original draft, writing—review and editing. A.K.B.: funding acquisition, investigation, methodology, project administration, resources, supervision, writing—original draft, writing—review and editing.

### Competing interests

The authors declare no competing interests.

### Additional information

**Supplementary information** The online version contains supplementary material available at <https://doi.org/10.1038/s41467-026-68698-5>.

**Correspondence** and requests for materials should be addressed to Aron K. Barbey.

**Peer review information** *Nature Communications* thanks Yaniv Assaf and the other, anonymous, reviewer(s) for their contribution to the peer review of this work. A peer review file is available.

**Reprints and permissions information** is available at <http://www.nature.com/reprints>

**Publisher's note** Springer Nature remains neutral with regard to jurisdictional claims in published maps and institutional affiliations.

**Open Access** This article is licensed under a Creative Commons Attribution-NonCommercial-NoDerivatives 4.0 International License, which permits any non-commercial use, sharing, distribution and reproduction in any medium or format, as long as you give appropriate credit to the original author(s) and the source, provide a link to the Creative Commons licence, and indicate if you modified the licensed material. You do not have permission under this licence to share adapted material derived from this article or parts of it. The images or other third party material in this article are included in the article's Creative Commons licence, unless indicated otherwise in a credit line to the material. If material is not included in the article's Creative Commons licence and your intended use is not permitted by statutory regulation or exceeds the permitted use, you will need to obtain permission directly from the copyright holder. To view a copy of this licence, visit <http://creativecommons.org/licenses/by-nc-nd/4.0/>.

© The Author(s) 2026

### Acknowledgements

We gratefully acknowledge the Human Connectome Project, WU-Minn Consortium (PIs: David Van Essen and Kamil Ugurbil) for collecting and providing the data analyzed in the main text of this publication. We also thank the INSIGHT investigators and project team for collecting the data analyzed in the Supplemental Materials. This project would not have been possible without the hard work of the numerous fellows, students, and staff that comprised such a fantastic research team. This research was funded by the Intelligence Advanced Research Projects Activity (IARPA), via Contract 2014-13121700004 to the University of Illinois at Urbana-Champaign (PI: Aron K. Barbey) and the Department of Defense, Defense Advanced Research Projects Agency (DARPA), via Contract